Original Article

MOLECULAR METABOLISM

Diminished ketone interconversion, hepatic TCA cycle flux, and glucose production in D-β-hydroxybutyrate dehydrogenase hepatocyte-deficient mice

David B. Stagg [1,2], Jacob R. Gillingham [1], Alisa B. Nelson [1,3], Justin E. Lengfeld [1], D. André d'Avignon [1], Patrycja Puchalska [1], Peter A. Crawford [1,2,3,*]

ABSTRACT

Objective: Throughout the last decade, interest has intensified in intermittent fasting, ketogenic diets, and exogenous ketone therapies as prospective health-promoting, therapeutic, and performance-enhancing agents. However, the regulatory roles of ketogenesis and ketone metabolism on liver homeostasis remain unclear. Therefore, we sought to develop a better understanding of the metabolic consequences of hepatic ketone body metabolism by focusing on the redox-dependent interconversion of acetoacetate (AcAc) and D-β-hydroxybutyrate (D-βOHB).
Methods: Using targeted and isotope tracing high-resolution liquid chromatography-mass spectrometry, dual stable isotope tracer nuclear magnetic resonance spectroscopy-based metabolic flux modeling, and complementary physiological approaches in novel cell type-specific knockout mice, we quantified the roles of hepatocyte D-β-hydroxybutyrate dehydrogenase (BDH1), a mitochondrial enzyme required for NAD^+/NADH-dependent oxidation/reduction of ketone bodies.
Results: Exogenously administered AcAc is reduced to D-βOHB, which increases hepatic NAD^+/NADH ratio and reflects hepatic BDH1 activity. Livers of hepatocyte-specific BDH1-deficient mice did not produce D-βOHB, but owing to extrahepatic BDH1, these mice nonetheless remained capable of AcAc/D-βOHB interconversion. Compared to littermate controls, hepatocyte-specific BDH1 deficient mice exhibited diminished liver tricarboxylic acid (TCA) cycle flux and impaired gluconeogenesis, but normal hepatic energy charge overall. Glycemic recovery after acute insulin challenge was impaired in knockout mice, but they were not more susceptible to starvation-induced hypoglycemia.
Conclusions: Ketone bodies influence liver homeostasis. While liver BDH1 is not required for whole body equilibration of AcAc and D-βOHB, loss of the ability to interconvert these ketone bodies in hepatocytes results in impaired TCA cycle flux and glucose production. Therefore, through oxidation/reduction of ketone bodies, BDH1 is a significant contributor to hepatic mitochondrial redox, liver physiology, and organism-wide ketone body homeostasis.

Keywords Mitochondrial redox homeostasis; Hepatic ketogenesis; Liver oxidative metabolism; Glucose metabolism; Metabolomics; Metabolic flux

1. INTRODUCTION

With rapidly emerging interest in exploiting intermittent fasting, ketogenic diets, and exogenous ketone therapies as prospective health-promoting, therapeutic, and performance-enhancing agents, the role of ketone metabolism and signaling in the liver remains relatively underexplored [1—5]. Hepatic ketogenesis, acting as an overflow for the hepatocyte TCA cycle, is a source of energy that is particularly engaged when carbohydrates are in short supply. Robust ketogenesis occurs through a fate-committing reaction catalyzed by the mitochondrial matrix enzyme 3-hydroxymethylglutaryl-CoA synthase (HMGCS2), which generates HMG-CoA from β-oxidation-derived acetoacetyl-CoA and acetyl-CoA [6]. After a lyase-dependent release of acetyl-CoA from HMG-CoA, the ketone body acetoacetate (AcAc) is formed; which is then reduced to D-β-hydroxybutyrate (βOHB) by the mitochondrial matrix enzyme D-βOHB dehydrogenase (BDH1) that catalyzes a near—equilibrium reaction requiring reduced (NADH) and generating oxidized (NAD^+) forms of nicotinamide adenine dinucleotide [7—9]. AcAc and D-βOHB are released into the circulation for extrahepatic terminal oxidation. Through mass action, mitochondrial BDH1 oxidizes D-βOHB back to AcAc, and mitochondrial succinyl-CoA-oxoacid transferase (SCOT, encoded by nuclear gene *Oxct1*) catalyzes the obligate fate-committing reaction ultimately converting AcAc to acetyl-CoA [10]. SCOT is a mitochondrial enzyme that transfers a CoA moiety to AcAc, supporting its ultimate conversion to acetyl-CoA, and is abundant in all mammalian mitochondria except those of hepatocytes

[1]Division of Molecular Medicine, Department of Medicine, University of Minnesota, Minneapolis, MN, USA [2]Department of Biochemistry, Molecular Biology, and Biophysics, University of Minnesota, Minneapolis, MN, USA [3]Bioinformatics and Computational Biology Program, University of Minnesota, Minneapolis, MN, USA

*Corresponding author. University of Minnesota, 401 East River Parkway, MMC 194, Minneapolis, MN 55455 USA. E-mail: crawforp@umn.edu (P.A. Crawford).

Received March 22, 2021 • Revision received May 28, 2021 • Accepted June 3, 2021 • Available online 8 June 2021

https://doi.org/10.1016/j.molmet.2021.101269

[6]. HMGCS2 is relatively restricted to hepatocytes, and thus, the liver is the only organ capable of contributing to the circulation of ketone bodies [11]. In contrast to the near-ubiquitous expression of SCOT, BDH1 expression varies among cell types [12]. BDH1 activity is greatest in the liver, with activities in the kidney, heart, brain, and skeletal muscle [7,13]. This variability in activity potentially relates to the unique role of BDH1 in catalyzing both the last step of ketogenesis (primarily hepatocytes) and the first step of ketone oxidation (extrahepatic tissues).

The liver plays a central role in equilibrating circulating AcAc and D-βOHB [14]. As the ratio of circulating AcAc/D-βOHB is directly proportional to the liver mitochondrial NAD^+/NADH ratio, BDH1 activity modulates mitochondrial redox potential [8,15]. With this in mind, any perturbations to the circulating ketone equilibrium, *i.e.,* exogenous ketones, could influence liver mitochondrial redox potential. To test this hypothesis, we generated a hepatocyte-specific BDH1-deficient mouse model. Using intersectional approaches in physiology and analytical biochemistry of static and dynamic metabolic signatures, we quantified the role of this hepatic ketone equilibration reaction on both liver and whole-body metabolism in the chow-fed and fasted states.

2. MATERIALS AND METHODS

2.1. Animals and diet

All animal experiments were approved by the Institutional Animal Care and Use Committee at the University of Minnesota. Hepatocyte-specific BDH1 knockout mice (KO) were generated by crossing *Bdh1*^{flox} mice [16] to mice expressing Cre recombinase under the control of the albumin promoter [17] and maintained for at least 10 generations on a C57BL/6NJ substrain hybrid background (Albumin-Cre X *Bdh1*$^{flox/flox}$). Littermate Cre-negative (*Bdh1*$^{flox/flox}$) mice were used as controls. Primer sequences used for genotyping are listed in Supplemental Table 1. Adult male and female mice (as identified in Results and Figure Legends) over the age of 12 weeks were used for all experiments. Mice were maintained on a standard low-fat chow diet (2016 Teklad global 16% protein rodent diet) and received autoclaved water ad libitum. A cohort of wild-type control mice was maintained on a 60% high-fat diet (D12492; Research Diets; 60% kcal fat, 20% protein, 20% carbohydrate). Mice were housed on corncob bedding in groups of 4 to 5 with lights off between 2000 and 0600 in a room maintained at 22°C. For fasting experiments, mice were housed on paper bedding with water provided ad libitum. Overnight, 18 h fast commenced at 1600 with experiments conducted at 1000 the next day. If mice were used for multiple studies, at least 1 week lapsed between experiments.

2.2. Exogenous delivery of ketones

Ethyl-acetoacetate (ethyl-AcAc) was obtained from Millipore Sigma (W241512). (R)-(−)-3-Hydroxybutyric acid sodium salt was obtained from Santa Cruz Biotechnology (sc-229,050). Ethyl-[U−$^{13}C_4$]AcAc and sodium D-[U−$^{13}C_4$]βOHB salt were purchased from Cambridge Isotope Laboratories (CIL, CLM-3297, and CLM-3853, respectively). AcAc and [U−$^{13}C_4$]AcAc were synthesized by the base-catalyzed hydrolysis of ethyl-AcAc or ethyl-[U−$^{13}C_4$]AcAc, respectively, as previously described [12]. To control for the equimolar quantity of ethanol produced in the synthesis of AcAc, equimolar quantities of ethanol were added to D-βOHB, D-[U−$^{13}C_4$]βOHB, and saline vehicle control preparations. Random-fed male mice received an intraperitoneal (i.p.) injection of unlabeled ketones at 10 μmol/g body weight or ^{13}C-labeled ketones at 1 μmol/g body weight. For circulating ketone assessments, serum was obtained before and at multiple time points post injection for ketone body quantification. For liver energy metabolite assessments, mice were sacrificed by cervical dislocation 15 min post ketone or vehicle injection, and livers were harvested and freeze-clamped within 15 s.

2.3. Serum ketone body quantification

Serum ketones were quantified using a method previously described by our group [18]. For serum or perfusion effluent (see Section 2.9) samples containing unlabeled ketones, 10 μL of diluted serum/perfusion effluent was extracted with 40 μL of cold 1:1 acetonitrile:methanol containing the internal standards [3,4,4,4-D_4]βOHB and [U−$^{13}C_4$]AcAc, both at 50 μM. Samples were vortexed and centrifuged at 4°C, 15,000×*g* for 10 min before analyzing the supernatant by UPLC-MS/MS. As this method uses [U−$^{13}C_4$]AcAc as an internal standard, it cannot be used to quantify serum levels of [U−$^{13}C_4$]AcAc. For samples containing ^{13}C-labeled ketones, first 4 μL of the internal standard [3,4,4,4-D_4]βOHB (50 μM) was added to 20 μL of diluted serum. Freshly prepared 24 μL of 1.8 M $NABD_4$ in 0.1 M NaOH was next added, resulting in the reduction of [U−$^{13}C_4$]AcAc present in the serum to [3-D_1,U−$^{13}C_4$]βOHB. After 5 min incubation at room temperature, 44 μL of acetonitrile was added and samples were vortexed. Following centrifugation at 4°C, 15,000×*g* for 10 min, samples were loaded into a cation exchange column, which was necessary to desalt the sample of excess Na^+, eluted in 3 mL of LC-MS grade water, and dried by SpeedVac. Dried samples were resuspended in 48 μL of 98% H_2O/2% methanol/0.0125% acetic acid, vortexed, and centrifuged at 4°C, 15,000×*g* for 10 min before analyzing the supernatant by UPLC-MS/MS.

2.4. Energy metabolite quantification

Frozen liver sections (weighed frozen) or mitochondrial pellets (quantified by protein content) were homogenized in 0.4 M perchloric acid, 0.5 mM EGTA extraction solution containing [$^{13}C_{10}$,$^{15}N_5$]ATP sodium salt (100 μM), [$^{13}C_{10}$,$^{15}N_5$]AMP sodium salt (100 μM), [1,2-$^{13}C_2$]acetyl-CoA lithium salt (5 μM), and [1,2,3-$^{13}C_3$] malonyl-CoA lithium salt (5 μM) purchased from Sigma. After incubation on ice for 10 min, samples were centrifuged at 15,000×*g* for 15 min at 4°C. The resulting supernatants were neutralized with freshly prepared 0.5 M K_2CO_3, vortexed, and centrifuged at 15,000×*g* for 30 min at 4°C. Final extracts were then analyzed by LC-MS/MS as previously described, with modifications [19]. Briefly, analysis of energy metabolites was performed using a Vanquish LC system. Separation was achieved on a reverse-phase C_{18} column (Waters Xbridge, 150 × 2.1 mm, 3 μm) using the following mobile phases: A) 95% water/5% methanol with 4 mM dibutylammonium acetate (DBAA, Millipore Sigma, 73,345) and B) 25% water/75% acetonitrile with 4 mM DBAA. The ion-pairing mobile phase additive DBAA provided for adequate chromatographic separation. Samples were separated using the following binary gradients: 0−80% B for 8 min, 80−100% B for 5 min, 100% B for 3 min, and 100−0% B for 5 min. The flow rate was 100 μL/min, with a diverter valve used for the first 2 min to minimize matrix components entering the MS. The column was maintained at 30°C and the injection volume was 2 μL. The LC system was hyphenated to a Thermo Q Exactive Plus MS equipped with heated electrospray ionization. The MS was operated in positive ionization mode with PRM mode used for quantitatively targeted analysis. The isolation window was set to *m/z* 1.0, resolution was 17,500, and collision energy 35 (arbitrary units). Retention times and *m/z* transitions for each metabolite are detailed in Supplemental Table 2.

2.5. Immunoblot

Protein extracts were prepared in a protein lysis buffer containing 20 mM Tris, 150 mM NaCl, 1 mM EDTA, 1% Triton-X 100, protease inhibitors (Roche), and phosphatase inhibitors (Sigma) as previously described [20]. Whole tissue protein lysates were prepared from frozen tissues and homogenized in ten times volume (microliters) to mass PLB. Protein targets of interest were probed with the following primary antibodies: HMGCS2 (Santa Cruz, Sc-33828), BDH1 (Atlas Antibodies, HPA030947), pAMPKα (Thr172), total AMPKα, pAKT (Ser473), and total AKT (Cell Signaling, 2535, 2532, 9271, and 9272, respectively). Horseradish peroxidase (HRP)-conjugated secondary antibodies included goat anti-rabbit IgG and goat anti-mouse IgG (Southern Biotech 4030—05 and 1015—05 respectively). Protein loading was assessed by BlotFastStain (G-Biosciences, 786—34), or by immunoblot against actin (Sigma A2066) and HRP-conjugated goat anti-rabbit IgG. Blots were developed using Immobilon Cresendo Western HRP substrate (Millipore Sigma, WBLUR0500) and imaged using a film or Bio-Rad ChemiDoc MP imaging system. Band intensities were densitometrically quantified using ImageJ software.

2.6. Histology and immunohistochemical staining

Following euthanasia by cervical dislocation, mouse liver sections were either fixed in 10% neutral buffered formalin or cryo-preserved in an OCT compound. Formalin tissue embedding, sectioning, and staining with hematoxylin and eosin was performed by the University of Minnesota Clinical and Translational Science Institute histology core. Frozen liver sections preserved in OCT were cut in 10 μm slices using a Leica CM1860 Cryostat at -20°C. Tissue sections were fixed on slides using 2% paraformaldehyde for 1 h, permeabilized for 20 min in 0.25% Triton-X 100, and blocked in 5% BSA/PBS/0.1% Triton-X 100 for 1 h. Rabbit anti-BDH1 (Atlas Antibodies, HPA030947) was incubated for 1 h at room temperature, followed by Alexa Fluor 488-conjugated goat anti-rabbit IgG (Invitrogen, A11008) for 30 min and mounted with Vectashield mounting medium with DAPI (Vector Laboratories, H1200). Primary and secondary antibodies were prepared in 5% BSA/1x PBS/0.1% Triton-X 100. Images were obtained using a Leica DM5500 B microscope.

2.7. Gene expression analysis

RNA was purified from liver or kidney lysates homogenized in RLT buffer (Qiagen) with 1% 2-mercaptoethanol using the RNeasy Mini Kit (Qiagen, 74,016) following the manufacturer's instructions. Reverse transcripts were generated using iScript (Bio-Rad, 170-8891) and real-time reverse-transcription polymerase chain reaction (RT-PCR) was performed using SsoAdvanced Universal SYBR Green Supermix (Bio-Rad, 172—5274) on a CFX384 Real-Time System (Bio-Rad). Transcripts were quantified using the $2^{-\Delta\Delta Ct}$ method. Liver and kidney transcripts were normalized to *Rpl32* and *Rna18s5,* respectively. Primer sequences used for gene expression are listed in Supplemental Table 3.

2.8. Serum measurements

Blood was acquired from submandibular bleed for fasting serum measurements. Blood glucose measurements were performed in duplicate using two CVS Health Advanced glucometers per collection, and the mean was taken. If the variance exceeded 10%, a third reading was noted and the outlier was removed. Nonesterified fatty acids (NEFA; Fujifilm, HR Series NEFA-HR2), triacylglycerols (TAG; Thermo Scientific, TR22421), and cholesterol (Fujifilm, 999—02601 and 993—02501) serum measurements were made using colorimetric assays following the manufacturer's instructions. ELISAs were used to measure serum insulin (Millipore Sigma, EZRMI-13K) and glucagon (Mercodia, 10—1271—01). All colorimetric assays were quantified using a Biotek Synergy HTX plate reader. HOMA-IR values were calculated as (Blood glucose (mg/dL) X Insulin (μU/mL)]/405) [21].

2.9. Metabolic flux studies

Portal vein perfusions were performed as previously described [22]. Briefly, mice were anesthetized with 50 μL of sodium pentobarbital (65 mg/mL, Vortech) administered i.p. Once they were fully unconscious and unresponsive to toe pinch (approximately 5 min following delivery), the portal vein was exposed and cannulated with a 24-gauge catheter needle, the abdominal aorta and inferior vena cava were cut, and the catheter was firmly tied into the portal vein. The beating heart was then exposed, and the right atrium was cut to prevent recirculation of buffer to the liver and to terminate perfusion to the brain. Livers were perfused with an oxygenated, glucose-free Krebs—Henseleit buffer, containing 3% $^{2}H_2O$, 0.1 mM sodium [U—$^{13}C_3$]propionate, 1.5 mM sodium lactate, 0.15 mM sodium pyruvate, and 0.25% glycerol, and unlabeled 0.2 mM sodium octanoate as an exogenous fat source. The buffer was prewarmed to 45°C (determined empirically to counter heat loss in tubing such that tissue delivery is maintained at physiological temperature) in a thermostat-controlled water bath. The buffer delivery was maintained at the rate of 8 mL/min using a peristaltic pump for 1 h. The perfusate effluent from the final 30 min of the procedure was collected and frozen for further processing. Hepatic oxidative fluxes were quantified using a ^{2}H-NMR and ^{13}C-NMR based approach as previously detailed [22,23] — by profiling monoacetone [$^{13}C/^{2}H$] glucose derived from hepatic venous effluent $^{13}C/^{2}H$-labeled glucose. ^{1}H-NMR, as previously described, was used to quantify total hepatic glucose and acetate production, octanoate consumption, and the uniformity of the perfusion procedure from separate perfusate effluent aliquots collected every 10 min. Perfusion effluent ketone bodies were quantified by LC-MS/MS as described in Section 2.3 to determine their rates of production. Acetyl-CoA estimation was performed by assuming that 4 mol of acetyl-CoA are produced from each mole of octanoate consumed. Each mole of βOHB, AcAc, and acetate produced consumed 2, 2, and 1 mol of acetyl-CoA, respectively, while each turn of the TCA cycle disposes 1 mol of acetyl-CoA. Reducing equivalents (RE) were estimated from fluxes as RE = (5.75 x TCA) + (3.5 x AcAc) + (2.5 x βOHB) + (1.75 x acetate) + (glycerol flux to glucose) — (0.1 x phospho*enol*pyruvate flux to glucose) [24].

2.10. Mitochondria isolation

Liver mitochondria were isolated as previously described [20]. Briefly, mice were sacrificed by cervical dislocation, livers harvested, and immediately homogenized in ice-cold mitochondrial isolation medium (MIM; 300 mM sucrose, 0.2 mM EDTA, 10 mM Na HEPES, BSA 1 mg/mL, pH 7.4). Homogenates were centrifuged at 600×*g* for 10 min at 4°C, and the resulting mitochondria-containing supernatant was further centrifuged at 8000×*g* for 15 min at 4°C. Mitochondrial pellets were resuspended in ice-cold MIM, aliquoted, and centrifuged again at 8000×*g* for 15 min at 4°C. Pellets were briefly washed in ice-cold MIM without BSA, then snap-frozen for downstream assays. Mitochondrial protein content was quantified by a BCA protein assay kit according to the manufacturer's instructions (Thermo Fisher 23,225).

2.11. NAD^+/NADH mass action ratio

For quantification of α-ketoglutarate and glutamate, frozen liver tissue was lyophilized and extracted as described previously [12], using cold (-20°C) 2:2:1 methanol:acetonitrile:H_2O containing an appropriate amount of the internal standard [U—$^{13}C_5$]glutamine (CIL). Extracted

liver samples were spiked with 20 mM ammonium phosphate to improve peak shape [25], then analyzed by LC/MS using Waters Acuity UPLC BEH Amide (130 Å, 1.7 μm, 2.1 mm × 150 mm) with the following mobile phases: A) 10 mM ammonium acetate and 10 mM ammonium hydroxide in 95% water, and B), 10 mM ammonium acetate and 10 mM ammonium hydroxide in 95% acetonitrile. Separation was performed using the following gradients: 100% B for 2 min, 100—30% B for 3 min, 30—20% B for 1.5 min, 20—30% B for 0.5 min, 30—100% B for 0.5 min, and 100% B for 2.5 min. Separation was carried out at the flow rate of 0.4 mL/min, column temperature 45°C, and sample injection volume of 4 μL. A Thermo Q Exactive Plus MS in PRM mode was used for quantitative targeted analysis. The mass spectrometer operated in negative ion mode with optimized HESI conditions: sheath gas 35, auxiliary gas 10, sweep gas 1, spray voltage 3.6, capillary temperature 275°C, S lens RF 50, and auxiliary gas temperature 150°C. For PRM mode, the AGC target was set to 2e5, while the resolution was set to 17,500. Retention times, *m/z* transitions, and optimal normalized collision energies [N(CE)] for each metabolite are detailed in Supplemental Table 4. The linearity between α-ketoglutarate or glutamate and internal standard was checked, and the correction factor was calculated based on three independently prepared calibration curves. Ammonia was quantified from frozen liver tissue by a colorimetric assay (Sigma, AA0100) according to the manufacturer's instructions. The mass action — NAD^+/NADH ratio — was then calculated as previously described [26].

2.12. Insulin and glucose tolerance tests

Blood glucose measurements were performed before and at regular intervals following i.p. insulin/glucose injection. For i.p. insulin tolerance tests (IPITT), male mice were administered i.p. Human insulin (Lilly, HI-213) at 0.75 U/Kg body weight for 18 h fasting tests, or 1 U/Kg bodyweight for 4 h fasting and random fed tests. For i.p. glucose tolerance tests (IPGTT), after fasting overnight (18 h), a bolus of a sterile-filtered glucose solution was delivered i.p. to female (2 mg glucose/g body weight) or male (1 mg glucose/g body weight) mice. The dosage of glucose for male mice was lowered because the 2 mg glucose/g body weight dose resulted in blood glucose readings outside the range of our glucometer.

2.13. Kidney lactate tracer experiment

Sodium lactate and sodium [U—$^{13}C_3$]lactate were purchased, respectively, from Millipore Sigma (L7022), and CIL (CLM-1579). Overnight-fasted male mice were administered [U—$^{13}C_3$]lactate (5 μmol/g body weight) by i.p. injection. Fifteen minutes post injection, mice were sacrificed by cervical dislocation, kidneys harvested, and rapidly freeze-clamped. Kidney tissue was lyophilized before extracting metabolites using cold (-20°C) 2:2:1 methanol:acetonitrile:H_2O. Kidney metabolites were then analyzed using the LC/MS parameters detailed in Section 2.11. Detected TCA metabolites were validated by the use of external standards. Thermo Quan Browser was used to integrate peaks manually using a mass tolerance of 5 ppm and retention time window of 30 s. All possible isotopologues were integrated. Metabolite enrichment was corrected for natural abundance using R package, IsoCorrectoR, as previously described [27].

2.14. Statistical analyses

Analyses were performed with GraphPad version 9.0.0 software (Prism, San Diego, CA) using tests described in the figure legends. P values describe comparisons between (or among) group means for measured values, accounting for the variances. Confidence intervals (CI, 95%) or percent differences within the text define the range spanning fold or percent differences between groups.

3. RESULTS

3.1. Distinct effects of exogenous AcAc versus D-βOHB on circulating ketones and liver redox

To determine the equilibration kinetics of exogenously delivered ketones, random fed, wild-type mice were injected with an intraperitoneal (i.p.) bolus of either AcAc, D-βOHB (both at 10 μmol/g bodyweight), or vehicle control. Tail bleeds were performed before injection and at regular intervals postinjection. Serum ketones were extracted and measured by LC-MS/MS using a recently developed method [18]. No differences in serum levels of AcAc, βOHB, or total ketone bodies (TKB) were observed before injections (compare the three panels of Supplemental Fig. 1A). At 15 min post injection, both AcAc and D-βOHB injected mice exhibited sharp increases in circulating TKB with minimal change in vehicle-injected mice (Figure 1A). Vehicle-injected mice exhibited a minimal increase in TKB at 60 min that dissipated by 120 min (note graph inset, left panel of Figure 1A), perhaps attributable to modest stress-induced lipolysis [28].

Injection of exogenous AcAc increased serum concentrations of both AcAc and βOHB, with βOHB concentrations surpassing those of AcAc by 30 min. In contrast, injection of exogenous D-βOHB predominantly increased serum βOHB levels, with only a minimal increase in serum AcAc. BDH1 catalyzes the NAD^+/NADH-dependent redox reaction responsible for the interconversion of AcAc and D-βOHB (Figure 1B), and equilibration of circulating ketones has been posed to occur exclusively in the liver [14]. Collectively, these results suggest two fates for circulating AcAc: (i) equilibration into the circulating D-βOHB pool and (ii) terminal disposal, largely by oxidation in extrahepatic tissues. Conversely, bolus-delivered D-βOHB does not readily equilibrate into the circulating AcAc pool, but is nonetheless rapidly and terminally disposed through oxidation in extrahepatic tissues. These findings are consistent with the K_{eq} of the reaction catalyzed by NAD^+/NADH-dependent BDH1, which favors D-βOHB production, but mass action can drive terminal oxidation of D-βOHB [8,9].

To determine whether the reduction of exogenously delivered AcAc to D-βOHB, and corresponding oxidation of NADH to NAD^+ could alter liver redox status, random fed, wild-type mice were injected with an i.p. bolus of AcAc, D-βOHB, or vehicle control. Fifteen minutes post injection, mice were sacrificed by cervical dislocation, and livers were immediately freeze-clamped for quantification of energy-related metabolites by LC-MS/MS. Livers of mice receiving exogenous AcAc presented a modest but nonstatistically significant increase (17.3 ± 7.2%, $p = 0.11$) in hepatic NAD^+ concentration over that of vehicle-treated controls, with a modest but nonstatistically significant decrease in NADH content, together leading to an increased NAD^+/NADH ratio (29.9 ± 6.2%, $p < 0.05$; Figure 1C). NAD^+ and NADH contents of the livers of mice injected with exogenous D-βOHB were not significantly different from vehicle controls, suggesting that exogenous AcAc, but not D-βOHB, can transiently alter liver redox status.

Pioneering studies [8,14,15,29] revealed the relationship among ketogenesis, mitochondrial redox, and liver metabolism. However, only preliminarily interventional testing of this relationship has been conducted, and it was not fully characterized in pathological states. Previous studies by our group and others have revealed that ketogenesis increases, when mice are maintained on a high-fat diet (HFD) [22,24]. However, humans with steatotic livers exhibit decreased ketogenesis and overall decreased equilibration between AcAc and D-βOHB in the

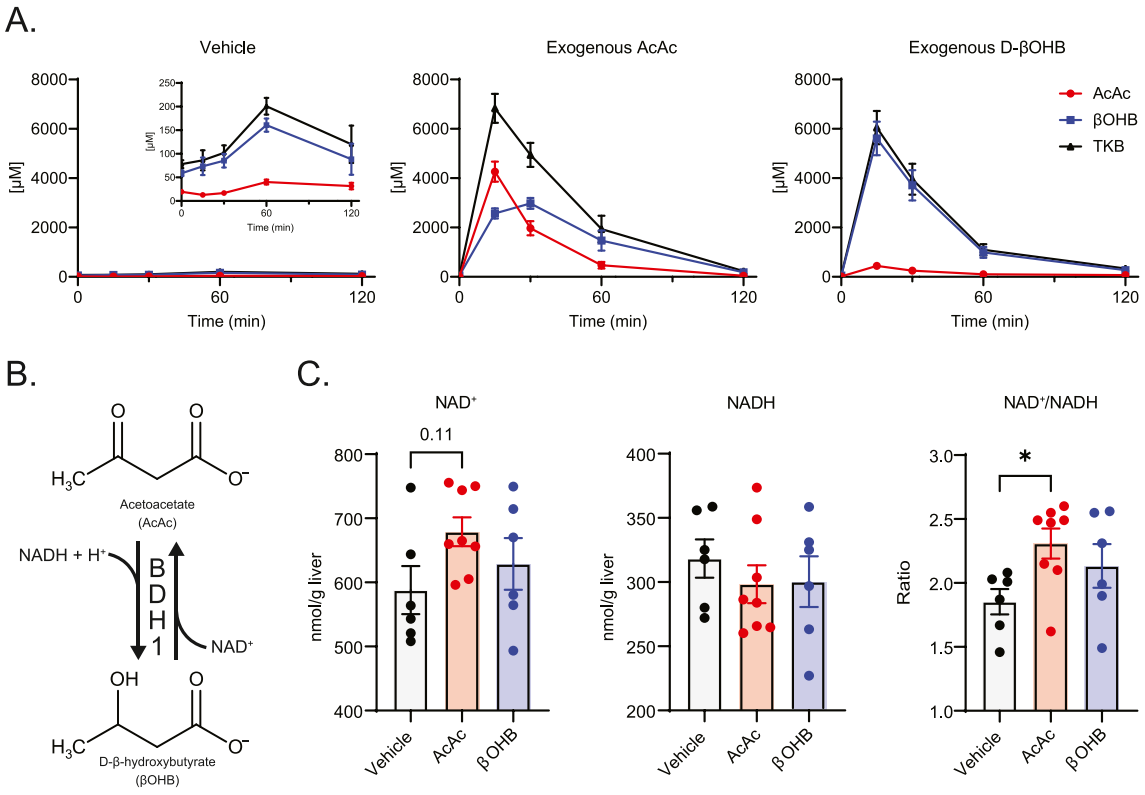

Figure 1: Effects of boluses of exogenous AcAc and D-βOHB on circulating ketones and liver redox. (A) Kinetic study of exogenously delivered AcAc (*middle*) and D-βOHB (*right*) turnover in random-fed C57BL/6NJ mice. Mice were injected i.p. [10 μmol/g body weight; vehicle was an equimolar concentration of ethanol vehicle] and blood was collected at the indicated time points (μM; $n = 5–10$/group). **(B)** Schematic of D-βOHB dehydrogenase 1 (BDH1) catalyzed interconversion of AcAc and D-βOHB. **(C)** Liver NAD^+ (nmol/g liver), NADH (nmol/g liver), and NAD^+/NADH ratio 15 min post exogenous ketone injections as described in **(A)** ($n = 6–8$/group). Data presented as mean ± SEM. $^*P < 0.05$ by one-way ANOVA with Tukey's multiple comparisons test.

fasting state [30]. To determine whether the expression of hepatic mediators of ketogenesis is dynamic in response to HFD, we quantified hepatic HMGCS2 and BDH1 protein abundances in 26-week-old wild-type mice maintained on either a chow diet or on a 60% HFD for 16 weeks. Although HMGCS2 expression remained unchanged with HFD treatment, BDH1 expression was significantly increased (Supplemental Figs. 1B—C). Whether dynamic expression of BDH1 is a cause, consequence, or bystander of altered ketone turnover is unclear. Therefore, in this study, to determine the role of hepatocyte BDH1 in liver physiology, we decided to study mice with hepatocyte-specific deficiency of this enzyme, focusing on male and female mice in the chow diet-fed and fasted states.

3.2. Generation of hepatocyte-specific BDH1 knockout mouse

Hepatocyte-specific BDH1 knockout mice (KO) were generated by crossing an Albumin-Cre strain [17] to a *Bdh1^{flox}* allele [16] maintained on a C57BL/6NJ background. Knockout of hepatic BDH1 was confirmed by hepatic protein (immunoblot and immunohistochemistry) and mRNA abundance (Figure 2A—C). Hepatocyte-BDH1-KO mice reached weaning at the expected Mendelian ratios (Supplemental Table 5). Hepatic BDH1 expression in both male and female KO mice was greatly reduced at 4 weeks of age and completely absent by 8 weeks (Supplemental Figs. 2A—B). Although the hepatic loss of BDH1 increased liver *Hmgcs2* mRNA abundance (Figure 2D), no differences in HMGCS2 protein expression were observed (Figure 2A, Supplemental Figs. 2A—B). Additionally, the knockout was specific to the liver with cardiac BDH1 expression in KO mice remaining intact (Figure 2E). Fasting body weights in 26-week-old mice were similar between control and KO mice, with no significant differences in fasting serum levels of triacylglycerols (TAG), nonesterified fatty acids (NEFA), or cholesterol for both sexes (Supplemental Figs. 3A—C). Additionally, no hepatic morphological differences were observed in hematoxylin and eosin-stained liver sections obtained from control and KO mice that were fasted for 18 h before tissue harvest (Supplemental Fig. 3D).

3.3. Hepatic BDH1 loss diminishes liver ketogenesis, but hepatic BDH1 is not required for systemic ketone equilibration

To determine the effect of hepatic BDH1 loss on circulating ketones, male and female mice were fasted 18 h, and serum was collected. Compared to littermate controls, serum AcAc levels were elevated by 38.9 ± 12.0% ($p < 0.05$) in KO mice (Figure 3A), whereas serum βOHB levels were diminished by 57.7 ± 8.5% ($p < 0.0001$), yielding a net decrease of 34.3 ± 9.9% ($p < 0.001$) in circulating TKB in KO mice. Similar circulating ketone alterations were observed in female mice fasted for 18 h (Supplemental Fig. 4A), in male mice fasted for 4 h (Supplemental Fig. 4B), and in random-fed mice of both sexes (Supplemental Figs. 4C—D), although the TKB decrease was less apparent in the fed state.

To determine the distribution of ketones produced by the liver, we next performed *ex vivo* portal vein perfusions in male KO and littermate control mice following an 18 h fast. Sixty-minute perfusions were conducted using an oxygenated, glucose-free Krebs—Henseleit buffer, containing unlabeled 0.2 mM sodium octanoate as an exogenous fat source. The hepatic venous effluent was collected and used for LC-MS/

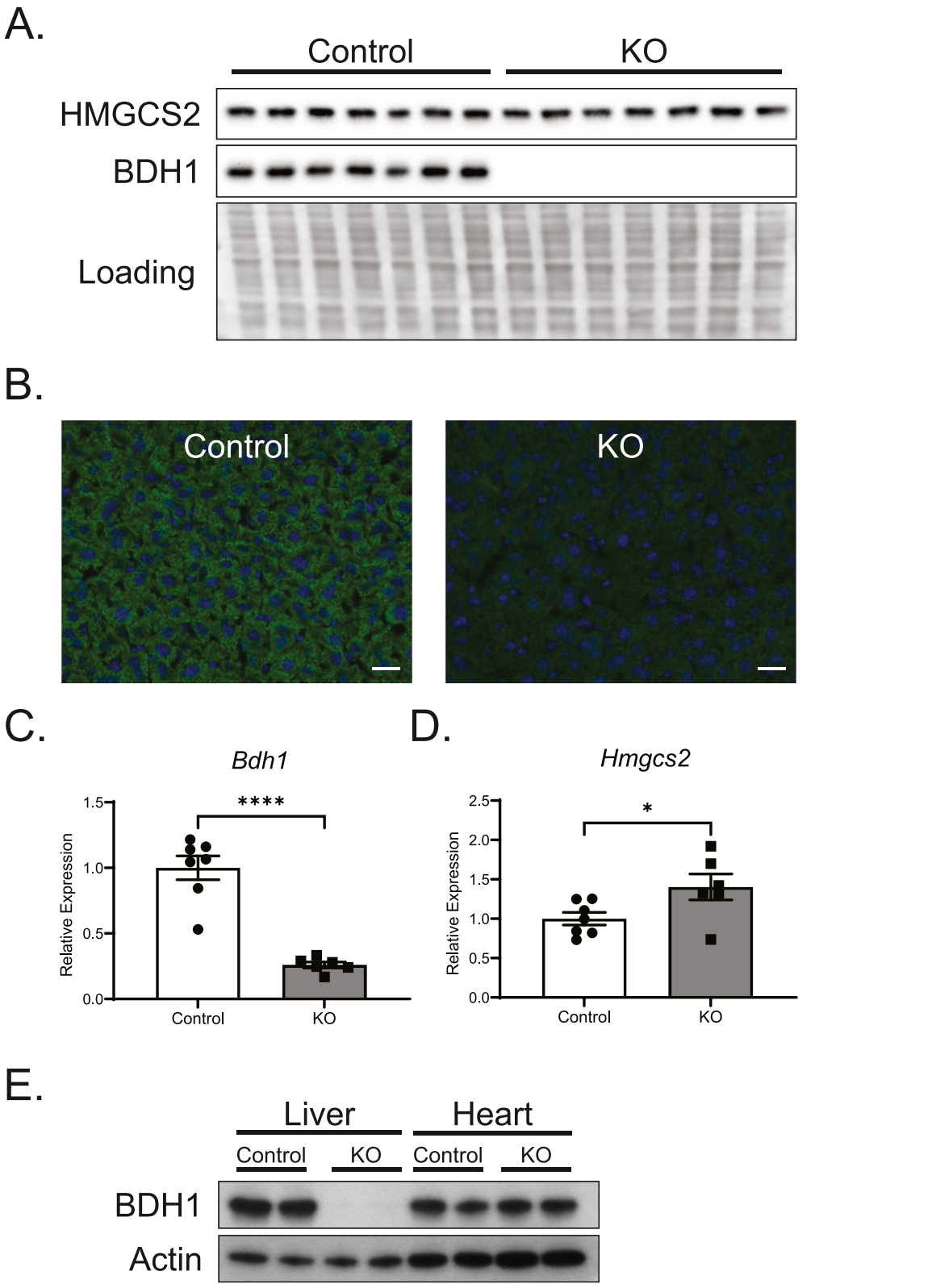

Figure 2: Confirmation of hepatocyte-specific BDH1-KO mice. (A) Immunoblots of HMGCS2, BDH1, and protein loading obtained from liver protein lysates of fasting littermate control (*Bdh1*$^{flox/flox}$) and hepatocyte-BDH1-KO (Albumin-Cre X *Bdh1*$^{flox/flox}$) mice ($n = 6$/group). **(B)** Representative 20× magnification of immunohistochemical stain for BDH1 in fasting liver cryosections. Scale bar = 25 μm. **(C)** Fasting liver transcript abundances of *Bdh1* and **(D)** *Hmgcs2* in control and KO mice ($n = 6–7$/group). **(E)** Immunoblots of BDH1 and Actin obtained from liver and heart protein lysates of fasting, male control and KO mice ($n = 2$/group). Data presented as mean ± SEM. $^{*}P < 0.05$; $^{****}P < 0.0001$ by Student's *t* test.

MS ketone quantification. Livers of KO mice produced AcAc at the rate of 2.3-fold (95% CI 1.8—3.0, $p < 0.0001$) greater than livers from littermate controls, while βOHB production was essentially zero at the rate of 0.04-fold (95% CI 0.03—0.05, $p < 0.0001$) than that of littermate controls (Figure 3B). The TKB production rate was diminished in the livers of KO mice at the rate of 0.7-fold (95% CI 0.6—0.9, $p < 0.05$) relative to littermate controls.

The very high [AcAc]/[βOHB] ratio in hepatic venous effluent [28.6 (± 2.5)-to-1] from livers of perfused KO mice (Figure 3B) was discordant from that of the circulating ketone pool [1.0 (± 0.1)-to-1] in these mice (Figure 3A). Conversely, hepatic venous effluents from perfused livers of littermate control mice exhibited [AcAc]/[βOHB] ratios [0.47 (± 0.04)-to-1] that were much more concordant with circulating ratios [0.32 (± 0.01)-to-1]. To test the hypothesis that extrahepatic equilibration of circulating ketones explains recovery of [AcAc]/[βOHB] ratios in the circulation of hepatocyte-BDH1-KO mice, we injected KO mice and their littermate controls (i.p.) with [U—$^{13}C_4$]AcAc (1 μmol/g body weight), and quantified the appearance of [U—$^{13}C_4$]βOHB in serum over time. Circulating [U—$^{13}C_4$]βOHB was detected at 10 and 20 min post injection in both control and KO [U—$^{13}C_4$]AcAc-treated mice, although [U—$^{13}C_4$]βOHB levels were 38.0 ± 12.8% ($p < 0.01$) and 41.6 ± 12.0% ($p < 0.01$) lower in KO mice, respectively (Figure 3C and Supplemental Fig. 4E). Similarly, following an injection of uniformly labeled D-[U—$^{13}C_4$]βOHB, circulating [U—$^{13}C_4$]AcAc was detected in both control and KO mice, with 36.6 ± 10.7% ($p < 0.01$) and 31.5 ± 9.6% ($p < 0.01$) lower conversion in KO mice at 10 and 20 min post injection (Figure 3D and Supplemental 4F). The kinetic responses to (Figure 3E) and fractional enrichments of (Supplemental Figs. 4G—H) exogenous ^{13}C-labelled ketones were concordant with the responses to unlabeled exogenous ketones (Figure 1A), with [U—$^{13}C_4$]AcAc readily reduced to [U—$^{13}C_4$]βOHB, but the oxidation product of exogenously delivered D-[U—$^{13}C_4$]βOHB, [U—$^{13}C_4$]AcAc, apparent in the circulation to a much lower extent in both KO and control mice.

Responses to exogenous ^{13}C-labeled ketones strongly suggest that extrahepatic tissues contribute to the equilibration of circulating ketones in the absence of hepatic BDH1, with only a modest deficiency. The hepatic loss of BDH1 increased kidney mRNA abundances for both *Bdh1* and *Hmgcs2* (Supplemental Figs. 5A—B), though no differences in abundances for the encoded proteins were observed (Supplemental Fig. 5C). The other theoretical source of AcAc/βOHB equilibration in the circulation is a non-BDH1-dependent hepatic enzyme, such as BDH2 [31], but this is highly unlikely, given the absence of any βOHB produced by perfused livers from hepatocyte-BDH1-KO mice.

3.4. Loss of hepatic BDH1 diminishes TCA cycle flux, anaplerosis, and phospho*enol*pyruvate sourced gluconeogenesis without altering liver energy charge

Loss of hepatocyte BDH1 induces a large increase in the mass action ratio of the reaction normally catalyzed by BDH1, [AcAc]/[βOHB], for ketones exported from the liver, from 0.47 in livers of littermate controls to 28.6 in the KO (Figure 3B). Application of the equilibrium constant for BDH1 (0.0493) would normally suggest a corresponding increase in mitochondrial NAD^+/NADH ratio, from ~10 to ~580, respectively, in response to this [AcAc]/[βOHB] ratio increase [26]. However, the absence of BDH1 prevents hepatic mitochondrial equilibration of the two ketones, and thus, abrogates a conduit for NADH reoxidation to NAD^+. Therefore, we quantified static concentrations of NAD^+ and NADH in the livers of mice fasted for 18 h, using an LC-MS/MS approach that quantifies these nucleotides against an authentic internal standard [19]. Intriguingly, no differences were observed between KO and control mice, either within isolated mitochondria or at the whole-tissue level (Figure 4A—B). Furthermore, the summed static concentrations of NAD^+ and NADH did not vary between KO and control mice in both isolated mitochondria (152.1 ± 21.9 vs. 163.9 ± 28.3 nmol/mg protein, respectively, $n = 6—9$ per group, $p = 0.75$) and whole liver tissue (1,133.4 ± 34.7 vs. 1,125.4 ± 27.7 nmol/g liver, respectively, $n = 10—12$ per group, $p = 0.86$). To further assess the effect of hepatocyte BDH1 loss on liver redox, we determined the mitochondrial NAD^+/NADH mass action ratio [26] from the products and reactants of the glutamate dehydrogenase system. No differences in whole liver tissue levels of α-ketoglutarate, glutamate, and ammonia were observed between KO and control mice (Figure 4C—D, Supplemental Fig. 6A), resulting in similar mass action NAD^+/NADH ratios of 1.3 ± 0.3 and 1.1 ± 0.2, respectively, compared to those determined by isolated mitochondria direct measurements of 1.1 ± 0.2 for KO mice and 1.4 ± 0.3 for control mice (Figure 4E).

The absence of a difference in static NAD^+ and NADH nucleotide concentrations in hepatic mitochondria and in whole liver tissue harvested from fasting mice lacking hepatocyte BDH1 and no differences in NAD^+/NADH ratios could be explained by several mechanisms that are not mutually exclusive. First, overall NAD^+/NADH equilibrium may be preserved by other matrix (mitochondria) and cellular (whole tissue) dehydrogenases, because BDH1 is one of the several mitochondrial matrix enzymes capable of reoxidizing NADH [8]. Second, the total nucleotide pool, much of which is protein-bound, may not reflect the free pool that is immediately accessible to matrix dehydrogenase enzymes, although measurement of the mass action ratio for the glutamate dehydrogenase system mitigates this concern [32]. A third possibility is that static NAD^+ and NADH concentrations do not reflect the electron exchange rates among redox reactions that determine turnover rates in oxidative metabolism, and thus, the absence of a difference in snapshot concentrations may not reflect an absence of NADH-dependent redox homeostasis. Because NAD^+ (and not $NADP^+$) is exclusively required to accept electrons from the intermediates α-ketoglutarate and malate, as hepatic fat is terminally oxidized in the TCA cycle, we hypothesized that loss of BDH1-dependent reoxidation of NADH could yield diminished TCA cycle flux owing to impaired bioavailability of matrix NAD^+. To test this hypothesis, *ex vivo* 60-min portal vein perfusions were performed on littermate control and hepatocyte-BDH1-KO mice following an overnight fast. Perfusions were performed using oxygenated Krebs—Henseleit buffer that lacked glucose, but contained unlabeled 0.2 mM sodium octanoate (exogenous fat source), flux tracers 3% ^2H_2O, and 0.1 mM sodium [U—$^{13}C_3$] propionate, and then, the hepatic venous effluent was collected. After quantification of total glucose production and octanoate consumption using ^{1}H-NMR, the hepatic ^{13}C/^{2}H—labeled glucose pool was extracted and converted to monoacetone glucose, from which ^{2}H and ^{13}C-NMR spectra were collected, allowing hepatic oxidative fluxes and glucose sourcing to be determined (schematized in Figure 5A) [22,33]. Indeed, TCA cycle flux in livers of KO mice was reduced to 0.3-fold (95% CI 0.2—0.6, $p < 0.01$) compared to that of littermate controls (Figure 5B) with corresponding decreases in the rates of anaplerosis, 0.5-fold (95% CI 0.3—0.8, $p < 0.01$, Figure 5C), and pyruvate cycling, 0.5-fold (95% CI 0.2—0.8, $p < 0.01$, Supplemental Fig. 6B). Total hepatic glucose production (HGP) was modestly, but not significantly, decreased in KO mice (Figure 5D) with nonsignificant decreases in both glycogenolysis and glycerol contributions to HGP (Supplemental Figs. 6C—D). As expected, given the diminution in TCA cycle flux, the contribution of phospho*enol*pyruvate (PEP, *i.e.,* TCA cycle-sourced) to HGP was decreased in KO mice to 0.5-fold (95% CI 0.3—0.8, $p < 0.01$) than that of littermate controls (Figure 5E). No differences in the rates of acetate production were observed between KO and control

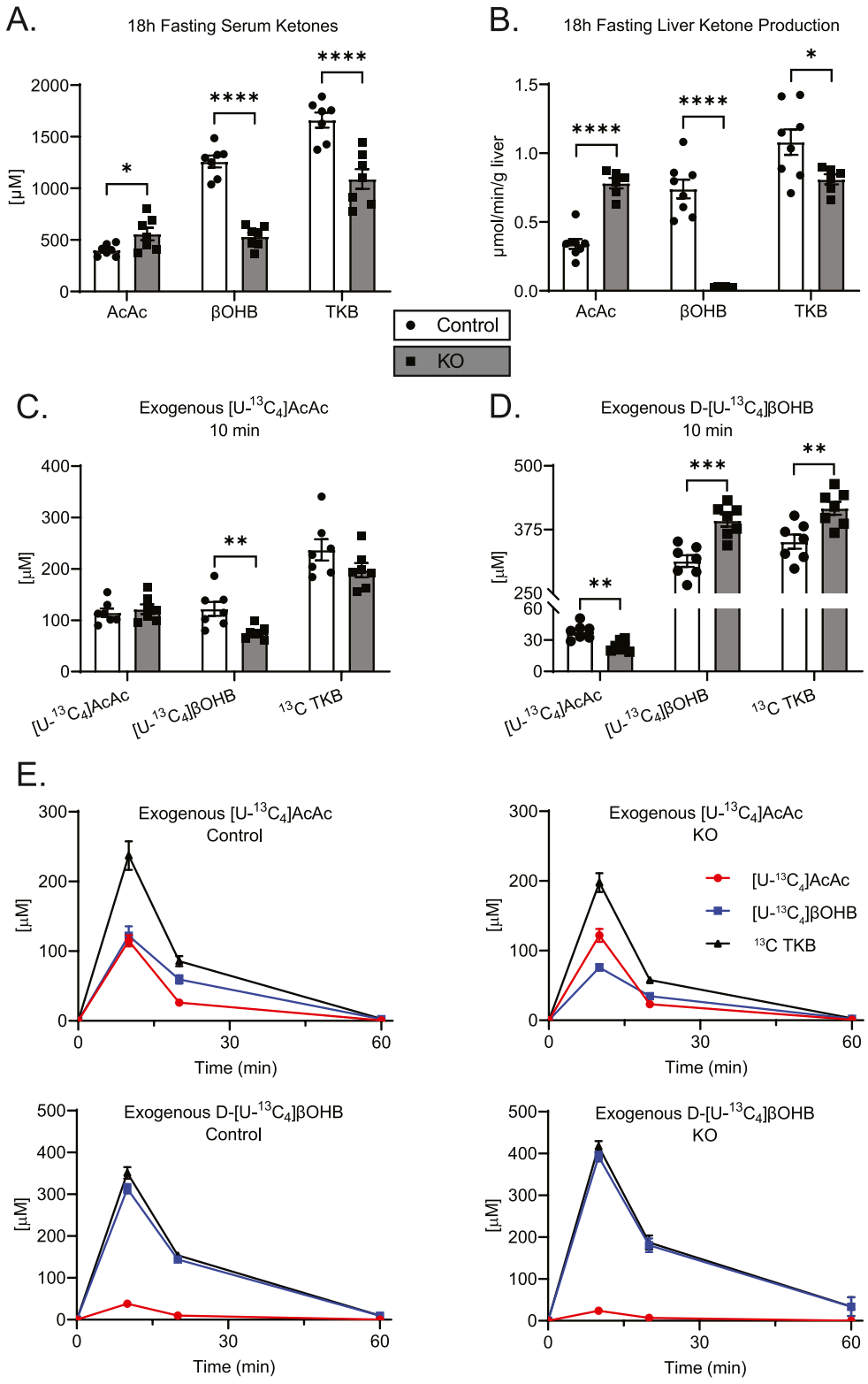

Figure 3: Hepatocyte-BDH1-KO mice exhibit impaired ketogenesis and ketone interconversion. (A) Fasting (18 h) serum ketones (μM; $n = 7$/group). **(B)** Liver ketone production, quantified by LC-MS of hepatic venous effluent from 60-min portal vein perfusion using an oxygenated buffer containing 0.2 mM unlabeled sodium octanoate as exogenous fat from 18 h fasted mice (μmol/min/g liver; $n = 6$–8/group). **(C)** Labeled circulating ketones (μM) 10 min post i.p. [U–$^{13}C_4$]AcAc or **(D)** D-[U–$^{13}C_4$]βOHB injection (1 μmol/g body weight) in random-fed control and KO mice ($n = 7$/group). **(E)** Full kinetics of [U–$^{13}C_4$]AcAc and D-[U–$^{13}C_4$]βOHB metabolism in random-fed control and KO mice. Mice were injected i.p. (1 μmol/g body weight) and blood was collected at the indicated time points ($n = 7$/group). The 10-min time points for this experiment are also presented in panels **(C–D)**. Twenty-minute time points are given in Supplemental Figs. 4E–F, and fractional contributions of all endogenous and exogenous ketones to the total pools are summarized in Supplemental Figs. 4G–H. Data presented as mean ± SEM. $^*P < 0.05$; $^{**}P < 0.01$; $^{***}P < 0.001$; $^{****}P < 0.0001$ by Student's *t* test.

mice (Figure 5F). Overall octanoate consumption was modestly diminished in livers of KO mice, but this difference did not reach a statistical significance (Figure 5G).

To determine whether there was evidence for an energy imbalance incurred by the loss of BDH1 in hepatocytes, the consumption rates of exogenously supplied octanoate were reconciled against the measured fates of octanoate oxidation, with the assumption that β-oxidation of 1 mol octanoate yields 4 mol acetyl-CoA. Terminal acetyl-CoA oxidation through the TCA cycle represented a minor fate (<1%) in control mice, and an even smaller fate for KO mice (<0.5%) for carbon available from octanoate-derived acetyl-CoA (Figure 5H). Acetate production subsumed a similar proportion of the carbon pool in both KO mice and controls; 29.2 ± 4.5% and 28.5 ± 2.0%, respectively. Proportionately, total ketogenesis was the major carbon product in both KO (60.6 ± 9.2%) and control (65.9 ± 2.0) mice. However, the fraction of the oxidized carbon pool delivered as AcAc was 58.4 ± 9.1% in KO, while it was 20.6 ± 0.6% in littermate controls ($p < 0.0001$). As storage of octanoate is minimal, unaccounted fates for oxidized octanoate, 10.0 ± 3.2% in KO, 5.2 ± 2.6% in littermate controls, are likely subsumed by incompletely oxidized intermediates, including short- and medium-chain acylcarnitines, or peroxisomal β-oxidation [34,35]. While flux through acetyl-CoA is very rapid and of high capacity during fat oxidation, static concentrations of acetyl-CoA are normally very low, and are thus a negligible contributor as a terminal fate of fat oxidation. Nonetheless, mitochondrial (but not whole liver) acetyl-CoA concentrations were increased 39.5 ± 9.9% ($p < 0.001$) in KO mice, with a corresponding 43.6 ± 17.5% ($p < 0.01$) diminution in mitochondrial succinyl-CoA concentrations (Figure 5I and Supplemental Fig. 6E), together with the impaired TCA cycle flux observation acquired using an orthogonal method. However, the overall estimated number of reducing equivalents (RE) produced did not differ between the genotypes, with 4.5 ± 0.2 RE generated in the hepatocyte-BDH1-KO liver, against 5.1 ± 0.4 RE in livers of littermate controls ($n = 6–8$ per group, $p = 0.22$). Thus, it was not surprising that mitochondrial and liver static tissue concentrations of ATP, ADP, and AMP, measured by LC-MS/MS using authentic internal standards from unperfused livers of fasting mice also did not exhibit differences between genotypes (Supplemental Figs. 6F–G). Moreover, no difference between total or phosphorylated hepatic AMPKα levels was observed in unperfused livers (Figure 5J). Nonetheless, significant increases in the abundances of *Ppargc1a* (1.53-fold, 95% CI 1.01–2.53, $p < 0.05$), *Pparg* (1.82-fold, 95% CI 1.20–2.76, $p < 0.01$), and *Pc* (1.57-fold, 95% CI 1.15–2.15, $p < 0.01$) mRNAs were detected in unperfused livers of fasting KO mice (Figure 5K). This upregulation might represent compensation for deficits in TCA flux and TCA cycle-sourced gluconeogenesis in KO mice. Given the subtle decrease in octanoate consumption in KO mice, increases in *Acadm* (1.47-fold, 95% CI 1.05–2.01, $p < 0.05$) and *Cpt2* (1.42-fold, 95% CI 1.06–1.87, $p < 0.05$) possibly represent upregulation of β-oxidation machinery. Additionally, though not relevant to the transport of medium-chain fatty acids used in the perfusion experiments, upregulation of *Lipc* and *Cd36* in livers of unperfused KO mice could represent compensation to increase triglyceride hydrolysis and fatty acid uptake, respectively (Supplemental Fig. 6H). No differences in *Acaca*, *Acacb*, *Acsl1*, or *Acsl3* expression between KO and control mice were observed. Changes in liver gene expression in KO mice could represent

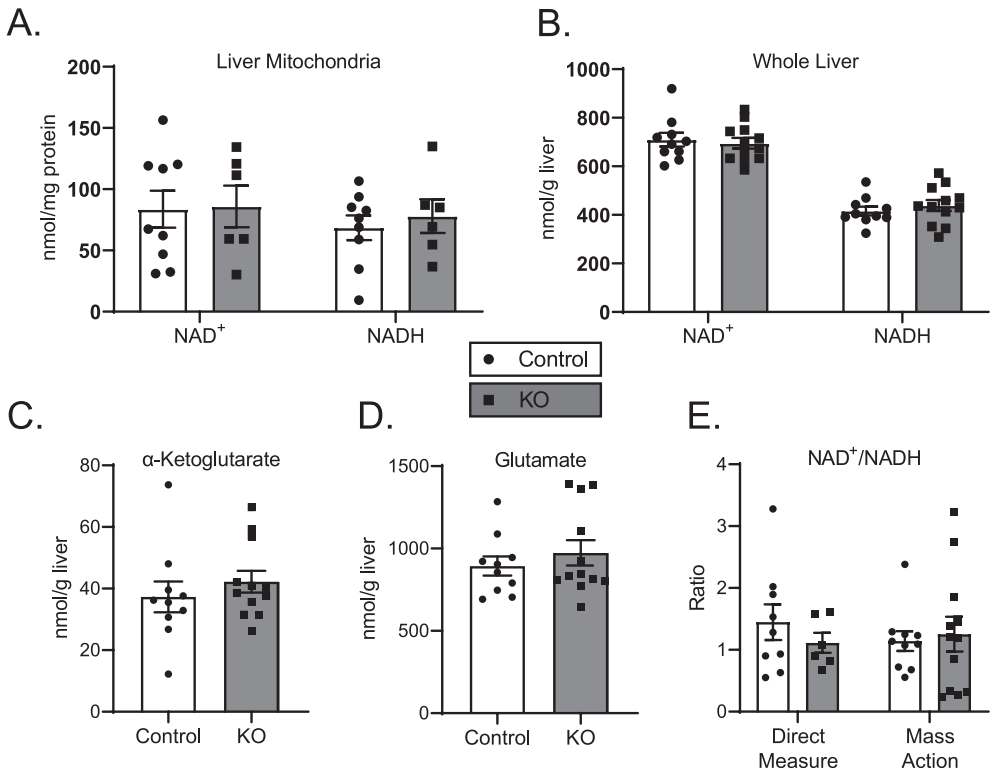

Figure 4: Hepatocyte-BDH1-KO mice maintain liver redox state. (A) LC-MS-determined static quantities of liver mitochondrial (nmol/mg protein) and **(B)** whole tissue (nmol/g liver) total NAD^+ and NADH in fasting (18 h) control and KO mice ($n = 6–12$/group). **(C)** Measured static quantities of liver α-ketoglutarate and **(D)** glutamate in fasting (18 h) control and KO mice (nmol/g liver, $n = 10–12$/group). **(E)** Liver mitochondrial NAD^+/NADH ratios determined from direct NAD^+ and NADH measurements from isolated mitochondria (*left*) and calculated from mass action ratio of glutamate dehydrogenase system from whole liver tissue (*right*) ($n = 6–12$/group). Data presented as mean ± SEM.

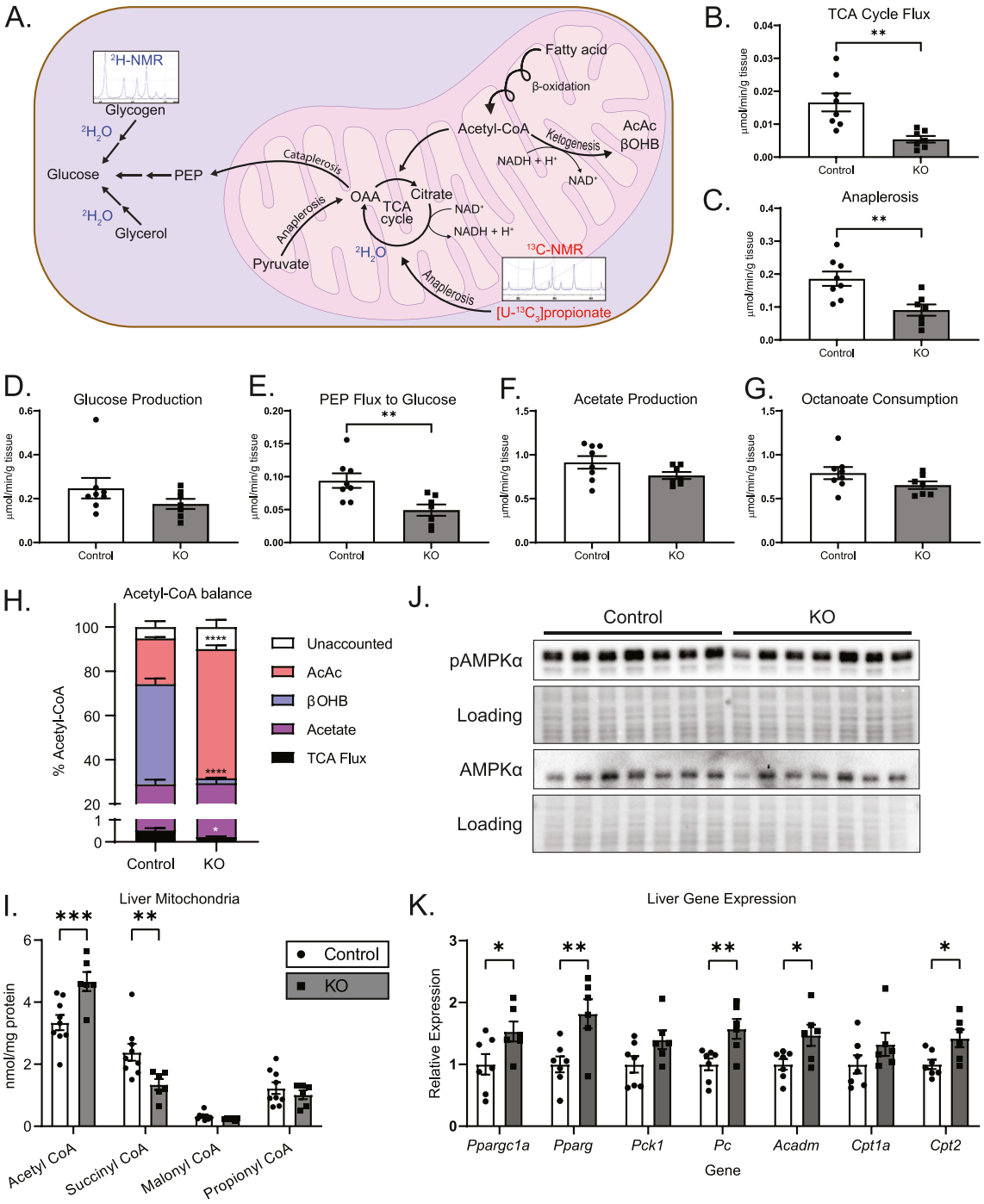

Figure 5: Loss of hepatic BDH1 diminishes hepatic oxidative fluxes. (A) Schematic highlighting hepatic oxidative fluxes obtained from liver perfusions using a ^{2}H-NMR and ^{13}C-NMR based approach. **(B)** TCA cycle flux, **(C)** anaplerosis flux, **(D)** hepatic glucose production, **(E)** phospho*enol*pyruvate (PEP)-supported (TCA cycle-sourced) flux to gluconeogenesis (glycogen- and glycerol-sourced fluxes to hepatic glucose production are given in Supplemental Figs. 6C–D), **(F)** acetate production, and **(G)** octanoate consumption rates, quantified by ^{13}C-, ^{2}H-, and ^{1}H-NMR, from perfusions, using an oxygenated buffer containing 0.2 mM unlabeled sodium octanoate, 3% $^{2}H_2O$, and 0.1 mM sodium [U−$^{13}C_3$]propionate in control and KO mice (µmol/min/g liver; $n = 7–8$/group). **(H)** Imputed balances of octanoate-derived acetyl-CoA fates based on measured disposal of acetyl-CoA through the TCA cycle and production of AcAc, βOHB, and acetate ($n = 6–8$/group). **(I)** Measured static quantities of liver mitochondrial (nmol/mg protein) total acetyl-CoA, succinyl-CoA, malonyl-CoA, and propionyl-CoA in fasting (18 h) unperfused control and KO mice ($n = 6–12$/group). **(J)** Immunoblots of phosphorylated AMPKα (pAMPKα), total AMPKα, and protein loading obtained from fasting (18 h) unperfused liver protein lysates of control and KO mice ($n = 7$/group). **(K)** Transcript abundances of *Ppargc1a*, *Pparg*, *Pck1*, *Pc*, *Acadm*, *Cpt1a*, and *Cpt2* from livers of fasting (18 h) unperfused control and KO mice. ($n = 6–7$/group). Data presented as mean ± SEM. $^{*}P < 0.05$; $^{**}P < 0.01$; $^{***}P < 0.001$ $^{****}P < 0.0001$ by Student's *t* test.

compensatory mechanisms to maintain energy homeostasis in the context of challenged redox control.

3.5. Hepatic loss of BDH1 alters whole-body glucose homeostasis

Given the impairment of TCA cycle-sourced gluconeogenesis in KO mice (Figure 5E), we next determined whether loss of hepatocyte BDH1 also affects whole-body glucose homeostasis. The 18 h fasting blood glucose levels in male KO mice were modestly, but not significantly, elevated over controls (Figure 6A). Fasting serum insulin and calculated HOMA-IR (Figure 6B–C) were also mildly elevated without statistical significance, with no change in fasting serum glucagon (Figure 6D). Measures of fasting glucose homeostasis were similar in female KO mice compared to their littermate controls, with no difference in fasting blood glucose (Supplemental Figs. 7A–D). Additionally, blood glucose levels in male KO mice starved for 48 h and female KO mice starved for 24 h were comparable to those of controls (Figure 6E–F). These data indicate no impairment of glycemic maintenance in the setting of starvation in mice lacking hepatic BDH1. To determine the ability of these mice to defend glycemia after an insulin challenge, we performed i.p. insulin tolerance tests (IPITT). The acute responses to insulin in both fed and 18 h fasting states were similar between male KO and littermate control mice (Figure 6G and Supplemental Fig. 7E). Additionally, liver Akt phosphorylation 15 min post insulin injection was comparable between KO and control mice, suggesting no effect of hepatic BDH1 loss on insulin sensitivity (Figure 7A). However, late recovery of blood glucose was impaired in KO mice 2 h post injection – either in those treated with i.p. insulin in the fed state, in which blood glucose levels relative to baseline were 23.0 ± 8.7% lower than those of littermate controls 2 h after insulin administration ($p < 0.05$, Figure 6G); or the 18 h fasted state, in which blood glucose levels relative to baseline were 28.3 ± 10.2% lower than those of littermate controls 2 h after insulin administration ($p < 0.01$, Supplemental Fig. 7E), together suggesting a modest defect in the ability of KO mice to return to normoglycemia after an insulin

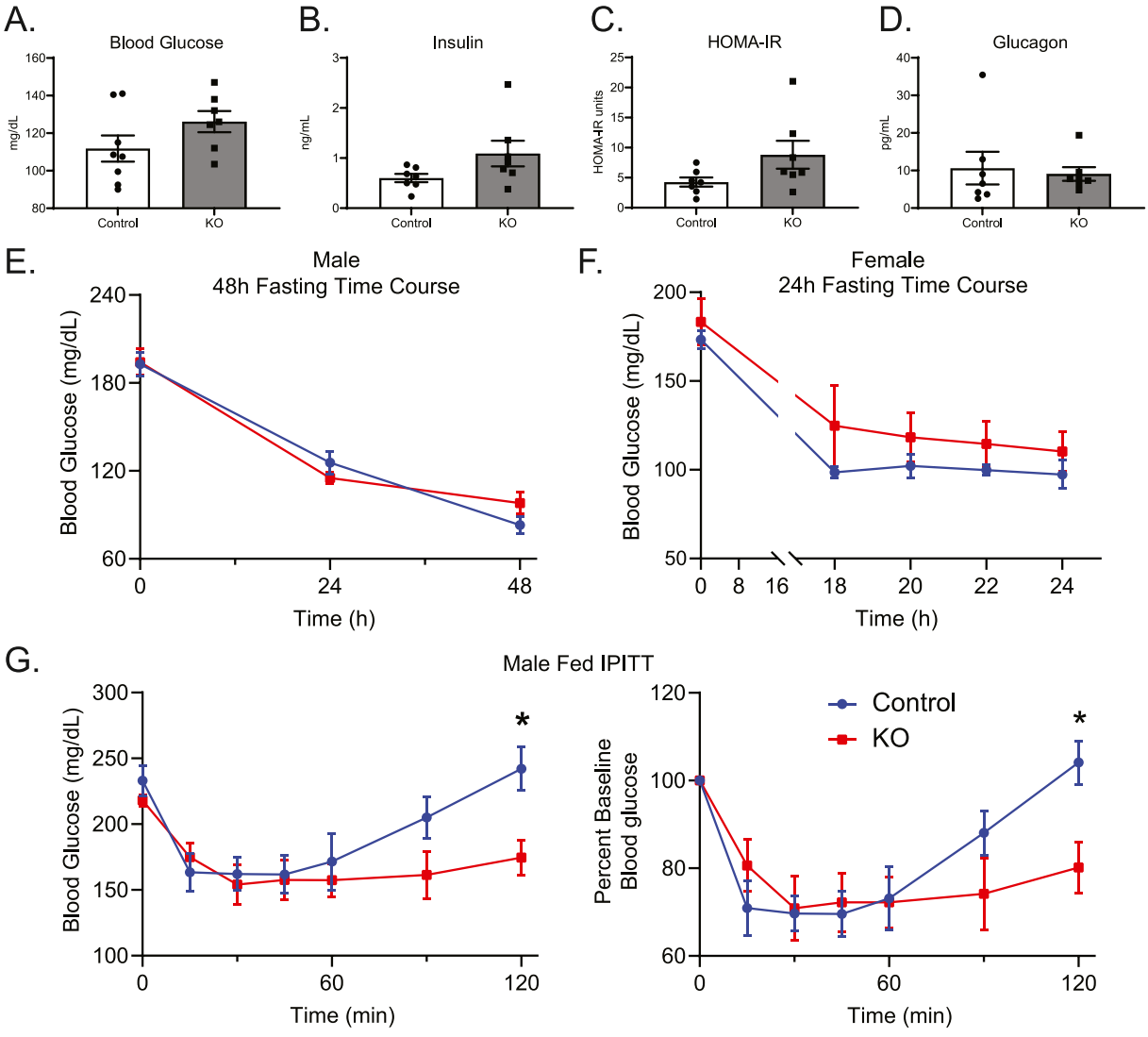

Figure 6: Altered glucose homeostasis in Hepatocyte-BDH1-KO mice. (A) Fasting serum measures of glucose (mg/dL), **(B)** insulin (ng/mL), **(C)** HOMA-IR, and **(D)** glucagon (pg/mL) in male control and KO mice ($n = 7–8$/group). **(E)** Blood glucose (mg/dL) time course in male control and KO mice during a 48 h starvation experiment ($n = 8$/group). **(F)** Blood glucose (mg/dL) time course in female control and KO mice during a 24 h starvation experiment ($n = 4$/group). **(G)** Random-fed IPITT (1 U/Kg body weight) with absolute and relative to baseline blood glucose curves ($n = 8$/group). Data presented as mean ± SEM. $^*P < 0.05$ by repeated-measures ANOVA with Sidak's multiple comparisons.

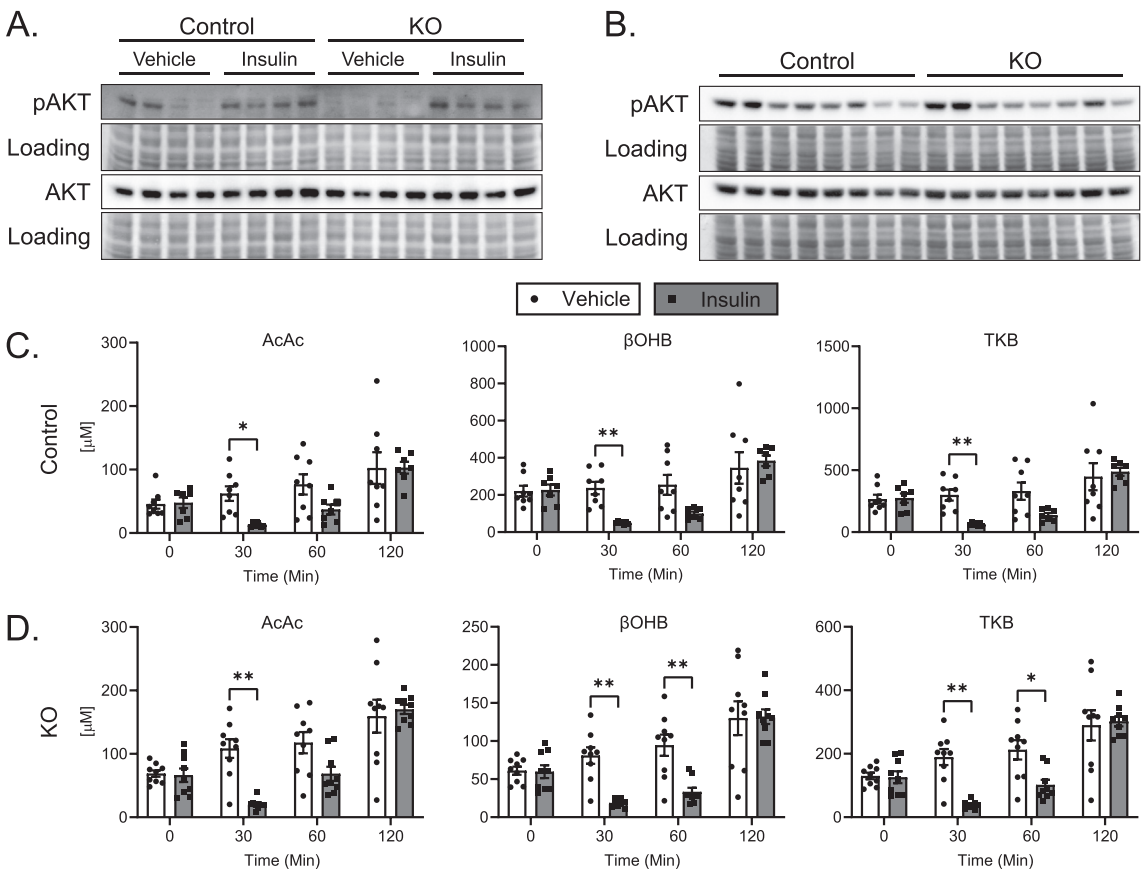

Figure 7: Hepatocyte-BDH1-KO mice remain insulin sensitive, with an intact ketone response to insulin. (A) Immunoblots of phosphorylated AKT (pAKT), total AKT, and protein loading obtained from 18 h fasting liver protein lysates of control and KO mice 15 min post insulin (0.75 U/Kg body weight) or saline vehicle injection ($n = 4$/group). **(B)** Immunoblots of pAKT, total AKT, and protein loading obtained from protein lysates of control and KO mice fasted for 4 h, injected with insulin (1 U/Kg body weight), then harvested 2 h post injection ($n = 8$/group). **(C)** Effect of insulin (1 U/Kg body weight) on circulating ketones in control and **(D)** KO mice ($n = 7–9$/group). The full kinetic course for these data are presented in Supplemental Fig. 8B. Data presented as mean ± SEM. $^*P < 0.05$; $^{**}P < 0.01$ by repeated-measures ANOVA with Sidak's multiple comparisons.

challenge. Biomarkers of insulin responsiveness, including liver Akt phosphorylation and circulating NEFA concentrations did not vary between KO and control mice 2 h post insulin injection (Figure 7B, Supplemental Fig. 8A).

To determine whether the relative impairment in glycemic defense after an insulin challenge in BDH1-hepatocyte-KO mice could be explained by enhanced insulin-mediated suppression of ketogenesis, and thus greater reliance of extrahepatic tissues on glucose, owing to less 'glucose sparing' [36], we quantified serum ketone concentrations in BDH1-hepatocyte-KO mice and littermate controls following i.p. administration of either insulin or saline control following a 4 h fast. In saline-treated mice of both genotypes, circulating ketone concentrations modestly increased over the 2 h period, consistent with the continued fast, from 4 to 6 h (Figure 7C–D, Supplemental Fig. 8B). However, in insulin-treated KO and control mice, circulating ketone concentrations sharply decreased after 30 min, but then recovered the same trajectory as that observed in saline-treated mice. By 2 h post injection, all ketone concentrations in insulin-treated mice, regardless of genotype, were comparable to saline-treated mice. Additionally, the total increase in TKB concentration over the 2 h period was similar between insulin-injected KO (176.2 ± 21.9 μM) and control (212.4 ± 38.0 μM) mice ($p = 0.40$). Taken together with similar NEFA concentrations 2 h post insulin administration (Supplemental Fig. 8A), these results indicate comparable degrees of insulin-mediated suppression of ketogenesis in mice lacking hepatic BDH1, with the normal recovery of circulating ketones. The comparable ability of the KO to recover ketogenesis following acute insulin suggests that latency to restore glycemia post insulin in these mice cannot be explained by increased extrahepatic glucose clearance owing to suppressed ketosis. However, impaired recovery of glycemia did correlate with impaired TCA cycle-sourced gluconeogenesis. If this gluconeogenic impairment exposes these mice to a risk for hypoglycemia, hepatic and/or extrahepatic mechanisms compensate for this deficiency during chronic hypoglycemic stress such as starvation. To assess glycemic excursion after an exogenous glucose load, we performed fasting (18 h) i.p. glucose tolerance tests (IPGTT). Although blood glucose levels were 20.2 ± 5.3% higher in male KO mice 15 min post glucose injection ($p < 0.05$), the overall area under the curve (AUC) did not exhibit differences between KO mice and controls in either male or female mice (Supplemental Figs. 9A–B).

Finally, as the kidney is a gluconeogenic organ [37], and because compensation through renal glucose production has been detected in another hepatocyte-specific knockout mouse model that impairs hepatic glucose production [38], we determined whether there was evidence of increased renal glucose production in heptocyte-BDH1-KO mice. Statistically significant ($p < 0.05$) fold increases in *Ppargc1a* [1.86-fold (95% CI 1.22–2.62) and *Pck1* (2.25-fold, 95% CI 1.23–3.95)], were noticed in kidneys harvested from fasting (18 h)

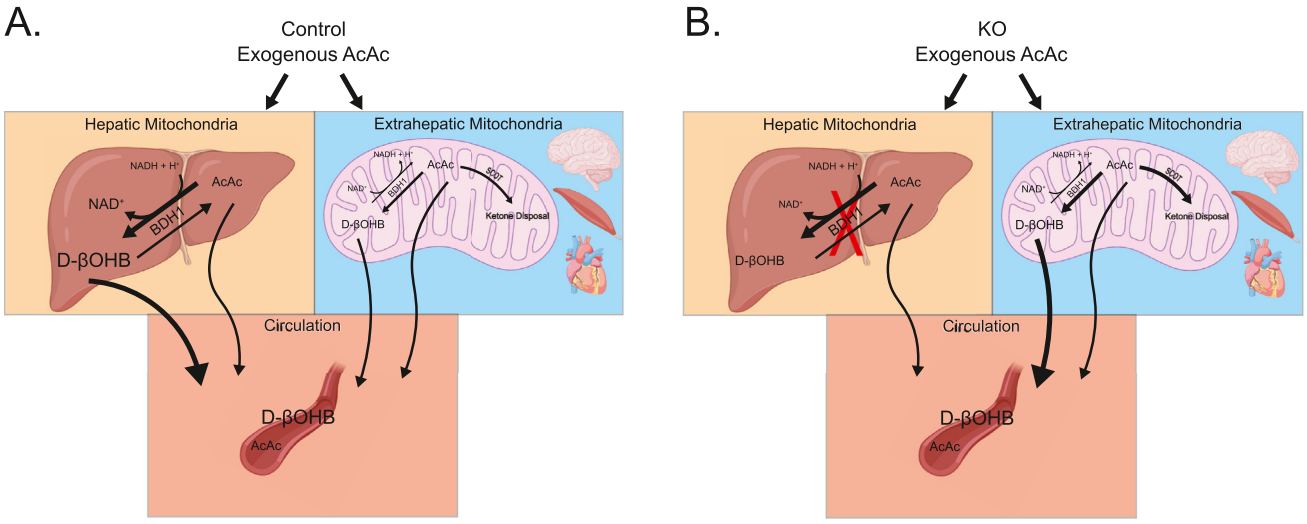

Figure 8: Summary of hepatocyte-specific BDH1-KO induced changes on ketone equilibration. (A) Schematic detailing the effect of an exogenous bolus of AcAc on circulating ketone equilibration in control and **(B)** KO mice. *In vivo*, liver mitochondrial NAD^+/NADH redox potential, ketone body mass action, and SCOT-dependent extrahepatic AcAc terminal oxidation together govern the circulating AcAc/D-βOHB ratio. The results provided here suggest that the governance of circulating AcAc/D-βOHB ratio is shared between hepatic and extrahepatic BDH1.

hepatocyte-BDH1-KO mice (Supplemental Fig. 10A) — suggesting increased fat oxidation, required for increased TCA cycle-sourced gluconeogenesis. To determine whether evidence for increased gluconeogenesis could be observed, we administered 5 μmol/g body weight [U—$^{13}C_3$]lactate i.p. to 18 h fasted mice and harvested kidneys 15 min later. Use of liquid chromatography high mass accuracy mass spectrometry study failed to detect evidence of increased ^{13}C-labeling of TCA cycle intermediates that would have suggested increased renal gluconeogenesis in hepatocyte-BDH1-KO mice (Supplemental Fig. 10B). However, renal mRNA abundances encoding mediators of glucose reabsorption after glomerular filtration, i.e., the glucose transporters *Slc2a1* [2.30-fold (95% CI 1.09—4.47), *Slc2a2* (2.17-fold, 95% CI 1.13—3.56), *Slc5a1* (2.66-fold, 95% CI 1.40—4.63), and *Slc5a2* (2.47-fold, 95% CI 1.36—4.30)], were all significantly ($p < 0.05$) elevated in the kidneys of hepatocyte-BDH1-KO mice (Supplemental Fig. 10C), suggesting a possible renal compensation to protect against hypoglycemia in hepatocyte-BDH1-KO mice.

4. DISCUSSION

Using high-resolution LC-MS/MS, dual isotope tracer NMR spectroscopy, and integrated physiological approaches in novel hepatocyte-specific BDH1 knockout mice, our results reveal new insight into the role of hepatic mitochondrial interconversion of the ketone bodies AcAc and D-βOHB. Rather than remaining in circulation until terminal ketolysis, much of the circulating AcAc pool is first reduced to D-βOHB in a BDH1-dependent manner by the liver and other BDH1-expressing tissues (schematized in Figure 8A). Although the reaction catalyzed by BDH1 is a near-equilibrium reaction, the equilibrium constant and midpoint reduction potential of the AcAc/D-βOHB half-reaction modestly favors D-βOHB and NAD^+ formation [8,9]. However, *in vivo*, mitochondrial redox potential, ketone body mass action, and SCOT-dependent extrahepatic AcAc terminal oxidation together govern the circulating AcAc/D-βOHB ratio [39]. The increase in static liver NAD^+/NADH ratios that were induced by exogenously administered AcAc underscores its two primary fates: SCOT-dependent extrahepatic oxidation and BDH1-dependent reduction to D-βOHB, in the liver and other BDH1 expressing tissues. Conversely, bolus-delivered D-βOHB did not as readily equilibrate in the circulation to the same extent as AcAc, and failed to reduce the hepatic NAD^+ pool, indicating that proportionately more of the D-βOHB pool was retained and terminally oxidized within the cells that oxidized it to AcAc. Thus, conversion of circulating AcAc to D-βOHB may target circulating AcAc to BDH1-expressing tissues, such as the brain, heart, and skeletal muscle. This could be physiologically significant, because while all extrahepatic cells express SCOT, BDH1 is not ubiquitously expressed [12].

In the fed state, the circulating [AcAc]/[D-βOHB] ratio is between 1:1 and 1:2, and this ratio decreases with progressively increasing physiological ketoses [8,26,40]. While it has been revealed that preferential extrahepatic disposal of AcAc may occur during ketosis, which explains this low ratio [14], our data suggest that while this may be true, equilibration of AcAc into the D-βOHB pool may also be a relatively favored process *in vivo*, a possibility supported by a recent study by Deja et al. [41]. A limitation of our approach was that bolus delivery may confer distinct equilibrium kinetics *in vivo* than infusions that achieve steady state concentrations, and these equilibria and their kinetics will vary by (patho)physiological state-dependent redox and substrate balances [14,42]. However, with respect to rapid infusions, understanding the impact of acute exogenous bolus ketone administration is highly relevant, given widespread interest in ketone ester formulations for prospective health and wellness applications, but that vary in their deliveries of D-βOHB or AcAc [1,43,44]. Another consideration is the circulating pool sampled, as the arterial [AcAc]/[D-βOHB] ratio more closely reflects hepatic mitochondrial NAD^+/NADH ratio than does venous [AcAc]/[D-βOHB] ratio. However, venous sampling provides a better index of whole-body equilibration between AcAc and D-βOHB. Moreover, in our experiments, portal venous perfusions provided direct insight into AcAc and D-βOHB exported from the liver.

These studies provide further insight into the tissue distribution of equilibrating circulating ketones. Fifty years ago, McGarry and Foster demonstrated that the liver was the primary site of equilibration

between AcAc and D-βOHB [14]. In that study, normal interconversion of exogenous AcAc or D-βOHB was nearly abolished in functionally hepatectomized rats. Our studies reveal that the liver is a primary site of ketone body equilibration, but extrahepatic organs contribute to ketone equilibration (schematized in Figure 8B). Residual hepatic BDH1 or theoretical compensation from hepatic cytoplasmic BDH2 [31] are unlikely explanations for the relative preservation of ketone body equilibration in hepatocyte-BDH1-KO mice, because when livers from these animals were perfused through the portal vein, only AcAc, and not βOHB was produced. This suggests that BDH2 does not have a role in ketone body-mediated redox homeostasis in the liver. Another possible explanation for the retention of ketone equilibration in the absence of hepatocyte BDH1 is that there is an extrahepatic compensation for the chronic absence of hepatic BDH1. For example, while *Bdh1* mRNA was elevated in kidneys of BDH1-hepatocyte-KO mice, BDH1 protein was not elevated (Supplemental Fig. 5). Nonetheless, future studies using a more acute deletion or inhibition of hepatocyte selective BDH1 can test whether adaptation of extrahepatic BDH1 occurs.

Hepatocyte-specific loss of BDH1 diminished total circulating ketone concentrations. Despite a modest increase in circulating AcAc, KO mice demonstrate decreases in both circulating βOHB and TKB levels in the fasting and to a lesser extent, fed states. These changes in circulating ketones are similar to those recently published in a total BDH1 knockout mouse model [45]. Although BDH1 is not the rate-limiting step in ketogenesis, our portal vein perfusion data indicate that this decrease in circulating ketones in KO mice reflects a modest decrease in overall hepatic ketogenesis. Perfusion studies revealed more AcAc being exported from the livers of KO mice than from the livers of littermate controls, while the majority of the AcAc produced by livers of control mice is reduced to D-βOHB before its export from the liver. Alternatively, but not mutually exclusive, the decrease in circulating ketone concentrations in hepatocyte-BDH1-KO mice could represent increased clearance by extrahepatic tissues. Clearance of all ^{13}C-labeled ketones (^{13}C-TKB) from mice administered [U—$^{13}C_4$]AcAc was more rapid in KO than in littermate control mice, whereas clearance of exogenously delivered D-[U—$^{13}C_4$]βOHB was relatively slower in the KO (Figure 3C—E and Supplemental Figs. 4E—F). In this experiment, the mild impairment in equilibration of [U—$^{13}C_4$]AcAc with the circulating pool of D-[U—$^{13}C_4$]βOHB in hepatocyte-BDH1-KO mice prospectively favors terminal disposal of [U—$^{13}C_4$]AcAc through SCOT-dependent pathways. However, the absence of hepatic interconversion of AcAc to βOHB may also support increased consumption of extrahepatic NADH by extrahepatic conversion to D-βOHB (Figure 8B). This could bear relevance to the relative latency to defend glycemia in the setting of an acute insulin challenge in mice lacking hepatic BDH1. While the kinetic responses of circulating ketones to insulin were comparable to those of littermate controls, serum AcAc concentrations were always modestly higher in the KO (Figure 7C—D, Supplemental Fig. 8B). NADH consumption through extrahepatic conversion of AcAc to βOHB possibly increases extrahepatic glucose disposal, although augmented glucose disposal was not evident in glucose tolerance tests. It is also of interest that after 48 h starvation, KO mice did not become more hypoglycemic than littermate controls. This suggests adaptation of mice lacking BDH1 in hepatocytes that overcomes a deficit in TCA cycle-sourced hepatic glucose production, possibly through extrahepatic glucose production/reclamation, and/or mechanisms that impair peripheral glucose uptake. Augmentation of a gene signature of energy turnover and re-uptake of filtered glucose in the kidney of hepatocyte-BDH1-KO mice are consistent with the former mechanism. Future direct interrogation of extrahepatic tissue metabolism in mice lacking hepatic BDH1 will add greater insight into the role of hepatic redox in the dynamic regulation of integrated glucose homeostasis — because these relationships are of great interest in the setting of ketogenic diets and exogenous ketone ester administrations.

We previously presented that ketogenic insufficiency provoked by the loss of hepatic HMGCS2 increases TCA cycle flux [22], which is the opposite outcome of the ketogenic defect incurred by BDH1 deficiency. With the loss of HMGCS2, acetyl-CoA cannot undergo ketogenesis, and there is proportionately more terminal oxidation in the TCA cycle. The different outcome observed in the livers of hepatocyte-BDH1-KO mice is likely based on the mitochondrial matrix redox implications of BDH1 loss, which the loss of HMGCS2 does not directly provoke. Without BDH1, liver mitochondria have lost a conduit to regenerate NAD^+ from NADH. Impairment in TCA cycle flux and the corresponding decrease in TCA cycle-sourced gluconeogenesis, both observed in livers of KO mice, results primarily in a consequence of this redox perturbation. It is also possible that without BDH1, liver mitochondria could retain more NADH, decreasing the demand for oxidative metabolism in the liver.

As BDH1 is one of the several mitochondrial dehydrogenases [8,26], loss of BDH1 in hepatocytes may provoke compensations that protect against more pronounced abnormalities of redox homeostasis: while hepatic TCA cycle flux was diminished in livers lacking BDH1, overall energy balance fell within normal limits, and energy charge, as measured by static abundances of ATP, ADP, and AMP, was normal. Mitochondrial and whole liver tissue redox status appeared to be normal, but as discussed in Results, static quantifications of total pools of NAD^+ and NADH encompass both free and protein-bound levels, which could mask a change in turnover rates [32]. Dynamic measurements of specific mitochondrial dehydrogenase activities against incrementally controlled variations of energy charge will be required to fully understand the redox effects of BDH1 loss on hepatocyte mitochondria, because exogenously administered AcAc does increase total liver NAD^+/NADH ratio, and the loss of BDH1 from hepatocytes provokes measurable changes in oxidative turnover rates.

Another consequence of ketogenic insufficiency is the loss of noncanonical signaling mechanisms conferred by ketone bodies. Metabolism-independent signaling roles of ketones may explain many of their physiological properties *in vivo* and should be considered prospective mechanisms to explain phenotypes in loss- or gain-of ketone turnover models or human participant studies [6]. AcAc and βOHB each confer distinct signaling effects through unique G protein-coupled receptor targets, components of the immune and inflammatory signaling systems, cytoplasmic signal transduction cascades, and post-translational histone modification. Differences between HMGCS2 and BDH1 loss of function models may be related to distinct signaling outcomes attributable to the loss of both AcAc and βOHB, versus the preservation of AcAc, and the relative loss of βOHB alone.

The perfused liver model employed herein confers an experimental limitation— as substrate delivery in this model does not reflect the physiological fatty acid supply sampled by hepatocytes *in vivo*, and also as the delivery of the carnitine palmitoyltransferase—independent fat octanoate in the livers of animals in the fasted state provokes a convergence of β-oxidation and ketogenic demand, not commonly encountered *in vivo*. This may overemphasize *in vivo* differences attributable to genetic perturbations of ketone metabolism, and result in variations among relative contributions to HGP, compared with those collected through *in vivo* studies. Nonetheless, the octanoate perfusion model was employed to specifically reveal the effect of deranged hepatic mitochondrial metabolism on downstream canonical glucose metabolism. Moreover, the portal vein perfusion model specifically

quantifies hepatic ketone export and HGP, unlike *in vivo* approaches that administer tracers through a central vein to track labeled glucose, which does not exclude extrahepatic gluconeogenesis.

In conclusion, equilibration of circulating ketones occurs primarily in the liver, but in the absence of hepatic BDH1, extrahepatic tissues support ongoing interconversion between the two ketone bodies in a manner that continues to favor the reduction of AcAc to D-βOHB with reoxidation of NADH. Additionally, hepatic loss of BDH1 diminishes the TCA cycle flux rate and provokes subtle changes in whole-body glucose homeostasis, but with a minimal overall effect on liver energy charge. Future studies that quantify the impact of hepatocyte BDH1 in varying metabolic contexts, such as nonalcoholic fatty liver disease, or in response to exogenous ketone body supplements, which provoke the unusual state of net ketone body import into hepatocyte mitochondria, may provide further insight into the roles of ketone body-governed mitochondrial redox homeostasis in metabolic physiology.

AUTHOR CONTRIBUTIONS

Conceptualization, D.B.S., D.A.D., P.P., and P.A.C.; Methodology, D.B.S., D.A.D., P.P., and P.A.C.; Investigation, D.B.S., J.R.G., A.B.N., J.E.L., D.A.D., and P.P.; Resources, P.A.C; Writing, Original draft, D.B.S., and P.A.C; Writing, reviewing, and editing, all authors; Visualization, D.B.S., and P.A.C; Supervision, P.A.C.; Funding Acquisition, P.A.C.

ACKNOWLEDGMENTS

The authors are grateful for support from NIH [DK091538, AG069781 (to P.A.C.) and T32 GM008244]. The authors thank Dan Kelly and Teresa Leone for kindly providing *Bdh1*^{flox} mice; Curtis Hughey for helpful conversations; Alisha Seay, Monica Sauer, and Eliana Pena for technical support. BioRender supported the construction of cartoon images.

CONFLICT OF INTEREST

P.A.C. has served as an external consultant for Pfizer, Inc., Abbott Laboratories, and Janssen Research & Development.

APPENDIX A. SUPPLEMENTARY DATA

Supplementary data to this article can be found online at https://doi.org/10.1016/j.molmet.2021.101269.

REFERENCES

[1] Stubbs, B.J., Cox, P.J., Evans, R.D., Santer, P., Miller, J.J., Faull, O.K., et al., 2017. On the metabolism of exogenous ketones in humans. Frontiers in Physiology 8(848).

[2] Cox, P.J., Kirk, T., Ashmore, T., Willerton, K., Evans, R., Smith, A., et al., 2016. Nutritional ketosis alters fuel preference and thereby endurance performance in athletes. Cell Metabolism 24(2):256—268.

[3] Veech, R.L., Bradshaw, P.C., Clarke, K., Curtis, W., Pawlosky, R., King, M.T., 2017. Ketone bodies mimic the life span extending properties of caloric restriction. IUBMB Life 69(5):305—314.

[4] Nielsen, R., Møller, N., Gormsen Lars, C., Tolbod Lars, P., Hansson Nils, H., Sorensen, J., et al., 2019. Cardiovascular effects of treatment with the ketone body 3-hydroxybutyrate in chronic heart failure patients. Circulation 139(18): 2129—2141.

[5] Yurista, S.R., Chong, C.R., Badimon, J.J., Kelly, D.P., de Boer, R.A., Westenbrink, B.D., 2021. Therapeutic potential of ketone bodies for patients with cardiovascular disease: JACC State-of-the-Art Review. Journal of the American College of Cardiology 77(13):1660—1669.

[6] Puchalska, P., Crawford, P.A., 2017. Multi-dimensional roles of ketone bodies in fuel metabolism, signaling, and therapeutics. Cell Metabolism 25(2):262—284.

[7] Lehninger, A.L., Sudduth, H.C., Wise, J.B., 1960. D-beta hydroxybutyric dehydrogenase of mitochondria. Journal of Biological Chemistry 235(8):2450—2455.

[8] Williamson, D., Lund, P., Krebs, H., 1967. The redox state of free nicotinamide-adenine dinucleotide in the cytoplasm and mitochondria of rat liver. Biochemical Journal 103(2):514—527.

[9] Krebs, H., Mellanby, J., Williamson, D., 1962. The equilibrium constant of the β-hydroxybutyric-dehydrogenase system. Biochemical Journal 82(1):96—98.

[10] Cotter, D.G., d'Avignon, D.A., Wentz, A.E., Weber, M.L., Crawford, P.A., 2011. Obligate role for ketone body oxidation in neonatal metabolic homeostasis. Journal of Biological Chemistry 286(9):6902—6910.

[11] Hegardt, F.G., 1999. Mitochondrial 3-hydroxy-3-methylglutaryl-CoA synthase: a control enzyme in ketogenesis. Biochemical Journal 338(Pt 3):569—582 (Pt 3.

[12] Puchalska, P., Martin, S.E., Huang, X., Lengfeld, J.E., Daniel, B., Graham, M.J., et al., 2019. Hepatocyte-macrophage acetoacetate shuttle protects against tissue fibrosis. Cell Metabolism 29(2):383—398 e387.

[13] Williamson, D.H., Bates, M.W., Page, M.A., Krebs, H.A., 1971. Activities of enzymes involved in acetoacetate utilization in adult mammalian tissues. Biochemical Journal 121(1):41—47.

[14] McGarry, J.D., Guest, M.J., Foster, D.W., 1970. Ketone body metabolism in the ketosis of starvation and alloxan diabetes. Journal of Biological Chemistry 245(17):4382—4390.

[15] Krebs, H.A., Wallace, P.G., Hems, R., Freedland, R.A., 1969. Rates of ketone-body formation in the perfused rat liver. Biochemical Journal 112(5):595—600.

[16] Horton, J.L., Davidson, M.T., Kurishima, C., Vega, R.B., Powers, J.C., Matsuura, T.R., et al., 2019. The failing heart utilizes 3-hydroxybutyrate as a metabolic stress defense. JCI Insight 4(4).

[17] Postic, C., Shiota, M., Niswender, K.D., Jetton, T.L., Chen, Y., Moates, J.M., et al., 1999. Dual roles for glucokinase in glucose homeostasis as determined by liver and pancreatic beta cell-specific gene knock-outs using Cre recombinase. Journal of Biological Chemistry 274(1):305—315.

[18] Puchalska, P., Nelson, A.B., Stagg, D.B., Crawford, P.A., 2021. Determination of ketone bodies in biological samples via rapid UPLC-MS/MS. Talanta 225: 122048.

[19] Fu, X., Deja, S., Kucejova, B., Duarte, J.A.G., McDonald, J.G., Burgess, S.C., 2019. Targeted determination of tissue energy status by LC-MS/MS. Analytical Chemistry 91(9):5881—5887.

[20] Schugar, R.C., Moll, A.R., André d'Avignon, D., Weinheimer, C.J., Kovacs, A., Crawford, P.A., 2014. Cardiomyocyte-specific deficiency of ketone body metabolism promotes accelerated pathological remodeling. Molecular Metabolism 3(7):754—769.

[21] Parks, B.W., Sallam, T., Mehrabian, M., Psychogios, N., Hui, S.T., Norheim, F., et al., 2015. Genetic architecture of insulin resistance in the mouse. Cell Metabolism 21(2):334—347.

[22] d'Avignon, D.A., Puchalska, P., Ercal, B., Chang, Y., Martin, S.E., Graham, M.J., et al., 2018. Hepatic ketogenic insufficiency reprograms hepatic glycogen metabolism and the lipidome. JCI Insight 3(12).

[23] Cotter, D.G., Ercal, B., Huang, X., Leid, J.M., d'Avignon, D.A., Graham, M.J., et al., 2014. Ketogenesis prevents diet-induced fatty liver injury and hyperglycemia. Journal of Clinical Investigation 124(12):5175—5190.

[24] Satapati, S., Kucejova, B., Duarte, J.A., Fletcher, J.A., Reynolds, L., Sunny, N.E., et al., 2015. Mitochondrial metabolism mediates oxidative stress

and inflammation in fatty liver. Journal of Clinical Investigation 125(12):4447—4462.

[25] Spalding, J.L., Naser, F.J., Mahieu, N.G., Johnson, S.L., Patti, G.J., 2018. Trace phosphate improves ZIC-pHilic peak shape, sensitivity, and coverage for untargeted metabolomics. Journal of Proteome Research 17(10):3537—3546.

[26] Krebs, H.A., Veech, R.L., 1969. Equilibrium relations between pyridine nucleotides and adenine nucleotides and their roles in the regulation of metabolic processes. Advances in Enzyme Regulation 7:397—413.

[27] Heinrich, P., Kohler, C., Ellmann, L., Kuerner, P., Spang, R., Oefner, P.J., et al., 2018. Correcting for natural isotope abundance and tracer impurity in MS-, MS/MS- and high-resolution-multiple-tracer-data from stable isotope labeling experiments with IsoCorrectoR. Scientific Reports 8(1):17910.

[28] Raje, V., Ahern, K.W., Martinez, B.A., Howell, N.L., Oenarto, V., Granade, M.E., et al., 2020. Adipocyte lipolysis drives acute stress-induced insulin resistance. Scientific Reports 10(1).

[29] Williamson, J.R., Scholz, R., Browning, E.T., 1969. Control Mechanisms of Gluconeogenesis and Ketogenesis: II. Interactions between fatty acid oxidation and the citric acid cycle in perfused rat liver. Journal of Biological Chemistry 244(17):4617—4627.

[30] Fletcher, J.A., Deja, S., Satapati, S., Fu, X., Burgess, S.C., Browning, J.D., 2019. Impaired ketogenesis and increased acetyl-CoA oxidation promote hyperglycemia in human fatty liver. JCI Insight 5(11):e127737.

[31] Guo, K., Lukacik, P., Papagrigoriou, E., Meier, M., Lee, W.H., Adamski, J., et al., 2006. Characterization of human DHRS6, an orphan short chain dehydrogenase/reductase enzyme: a novel, cytosolic type 2 R-beta-hydroxybutyrate dehydrogenase. Journal of Biological Chemistry 281(15):10291—10297.

[32] Veech, R.L., Todd King, M., Pawlosky, R., Kashiwaya, Y., Bradshaw, P.C., Curtis, W., 2019. The "great" controlling nucleotide coenzymes. IUBMB Life 71(5):565—579.

[33] Deja, S., Fu, X., Fletcher, J.A., Kucejova, B., Browning, J.D., Young, J.D., et al., 2020. Simultaneous tracers and a unified model of positional and mass isotopomers for quantification of metabolic flux in liver. Metabolic Engineering 59:1—14.

[34] Violante, S., Achetib, N., Roermund, C.W.T., Hagen, J., Dodatko, T., Vaz, F.M., et al., 2019. Peroxisomes can oxidize medium- and long-chain fatty acids through a pathway involving ABCD3 and HSD17B4. The FASEB Journal 33(3):4355—4364.

[35] Bian, F., Kasumov, T., Thomas, K.R., Jobbins, K.A., David, F., Minkler, P.E., et al., 2005. Peroxisomal and mitochondrial oxidation of fatty acids in the heart, assessed from the 13C labeling of malonyl-CoA and the acetyl moiety of citrate. Journal of Biological Chemistry 280(10):9265—9271.

[36] Al Batran, R., Gopal, K., Capozzi, M.E., Chahade, J.J., Saleme, B., Tabatabaei-Dakhili, S.A., et al., 2020. Pimozide alleviates hyperglycemia in diet-induced obesity by inhibiting skeletal muscle ketone oxidation. Cell Metabolism 31(5):909—919 e908.

[37] Krebs, H.A., Speake, R.N., Hems, R., 1965. Acceleration OF renal gluconeogenesis BY ketone bodies and fatty acids. Biochemical Journal 94(3):712—720.

[38] Cappel, D.A., Deja, S., Duarte, J.A.G., Kucejova, B., Inigo, M., Fletcher, J.A., et al., 2019. Pyruvate-carboxylase-mediated anaplerosis promotes antioxidant capacity by sustaining TCA cycle and redox metabolism in liver. Cell Metabolism 29(6):1291—1305 e1298.

[39] Cotter, D.G., Ercal, B., d'Avignon, D.A., Dietzen, D.J., Crawford, P.A., 2013. Impact of peripheral ketolytic deficiency on hepatic ketogenesis and gluconeogenesis during the transition to birth. Journal of Biological Chemistry 288(27):19739—19749.

[40] Cahill Jr., G.F., 2006. Fuel metabolism in starvation. Annual Review of Nutrition 26:1—22.

[41] Deja, S., Kucejova, B., Fu, X., Browning, J.D., Young, J.D., Burgess, S., 2021. In vivo estimation of ketogenesis using metabolic flux analysis—technical aspects and model interpretation. Metabolites 11(5).

[42] Miles, J.M., Schwenk, W.F., McClean, K.L., Haymond, M.W., 1986. A dual-isotope technique for determination of in vivo ketone body kinetics. American Journal of Physiology 251(2 Pt 1):E185—E191.

[43] Mujica-Parodi, L.R., Amgalan, A., Sultan, S.F., Antal, B., Sun, X., Skiena, S., et al., 2020. Diet modulates brain network stability, a biomarker for brain aging, in young adults. Proceedings of the National Academy of Sciences 117(11):6170—6177.

[44] D'Agostino, D.P., Pilla, R., Held, H.E., Landon, C.S., Puchowicz, M., Brunengraber, H., et al., 2013. Therapeutic ketosis with ketone ester delays central nervous system oxygen toxicity seizures in rats. American Journal of Physiology - Regulatory, Integrative and Comparative Physiology 304(10): R829—R836.

[45] Otsuka, H., Kimura, T., Ago, Y., Nakama, M., Aoyama, Y., Abdelkreem, E., et al., 2020. Deficiency of 3-hydroxybutyrate dehydrogenase (BDH1) in mice causes low ketone body levels and fatty liver during fasting. Journal of Inherited Metabolic Disease 43(5):960—968.

